APPLIED SCIENCES AND ENGINEERING

Nanoengineered mesenchymal stem cell therapy for pulmonary fibrosis in young and aged mice

Meng-Meng Han[1]†, Xing-Yue He[1]†, Ling Tang[1]†, Liang Qi[2], Ming-Yuan Yang[1], Yi Wang[1,3], Lei Xing[1,3], Jee-Heon Jeong[4], Hu-Lin Jiang[1,3,5]*

Pulmonary fibrosis (PF) is an age-related interstitial lung disease that results in notable morbidity and mortality. The Food and Drug Administration–approved drugs can decelerate the progression of PF; however, curing aged patients with severe fibrosis is ineffective because of insufficient accumulation of these drugs and wide necrocytosis of type II alveolar epithelial cells (AEC IIs). Here, we constructed a mesenchymal stem cell (MSC)–based nanoengineered platform via the bioconjugation of MSCs and type I collagenase–modified liposomes loaded with nintedanib (MSCs-Lip@NCAF) for treating severe fibrosis. Specifically, MSCs-Lip@NCAF migrated to fibrotic lungs because of the homing characteristic of MSCs and then Lip@NCAF was sensitively released. Subsequently, Lip@NCAF ablated collagen fibers, delivered nintedanib into fibroblasts, and inhibited fibroblast overactivation. MSCs differentiated into AEC IIs to repair alveolar structure and ultimately promote the regeneration of damaged lungs in aged mice. Our findings indicated that MSCs-Lip@NCAF could be used as a promising therapeutic candidate for PF therapy, especially in aged patients.

INTRODUCTION

Pulmonary fibrosis (PF) is an insidious and fatal lung disorder characterized by declining pulmonary function. PF usually occurs in aged people and has a median survival time of 2 to 3 years after diagnosis (*1*, *2*). It is characterized by type II alveolar epithelial cells (AEC IIs) injury, which is accompanied by the overactivation of fibroblasts and excessive extracellular matrix (ECM) accumulation (*3*). Nintedanib (NIN) and pirfenidone (PFD), Food and Drug Administration–approved therapeutics, can decelerate the progression of this disease to some extent, but they do not notably extend the median survival time of patients in clinic (*4*, *5*). This deficiency is probably due to low drug delivery efficiency to the lungs and the absence of injured AEC IIs repair (*6*, *7*).

With the rapid development of materials science, various nanocarriers have been widely studied for the treatment of intractable diseases (*8*). Recent therapeutic strategies have achieved favorable curative effects against PF in young mice by regulating fibroblasts and immune cells (*9*–*12*). However, these nanocarriers are often endocytosed and eliminated as "non-self" substances in the systemic circulation, and only a few nanoparticles enter target cells (*13*). To further improve the targeting efficiency and enhance drug accumulation, we prepared polymeric micelles loaded with two drugs (PER NPs) adhered to monocyte-derived multipotent cell (MOMC) to form MOMC/PER, which exhibited excellent effects against PF in young mice (*14*). However, PF is a quintessential age-related disease with a median diagnosis age of 66 years, and aged patients with severe fibrosis tended to become more refractory because of widely necrotic AEC IIs and compact ECM deposition within fibrotic lungs (*15*–*18*). Therefore, it is urgent to seek an effective therapeutic strategy for treating PF in aged patients.

As the basic structural and functional units of the organism, cells can be used as promising drug carriers for their inherent advantages, such as robust biocompatibility and the ability to escape from the reticuloendothelial system (*19*, *20*). During the progression of PF, injured AEC IIs continuously release chemotactic factors to recruit and guide mesenchymal stem cells (MSCs) to injured lung tissue (*21*, *22*). In addition, MSCs can differentiate into AEC IIs to participate in reestablishing lung function and secrete cytokines to repair injured AEC IIs (*23*, *24*). Therefore, MSCs can serve as promising delivery platforms to improve lung-targeting specificity (*25*). On the other hand, type I collagenase can specifically hydrolyze the three-dimensional helical structure of collagen fibers, making it more susceptible to proteolytic enzymes (*26*). In our previous study, type I collagenase decoration facilitated collagen fiber degradation and improved intracellular uptake (*27*, *28*). Thus, the surface of MSCs was designed to carry synthetic nanoparticles that could penetrate the collagen barrier and target overactivated fibroblasts.

Here, we first examined the course of PF in young and aged mice. Aged mice developed more severe fibrotic pathological features than young mice. Then, NIN was intragastrically administrated to investigate discrepancies in its curative effects on young and aged mice. NIN exerted considerable efficacy against PF in young mice but had negligible therapeutic effects on aged mice. Thus, we constructed an MSC-based nanoengineered therapeutic platform via the bioconjugation of MSCs and type I collagenase–modified liposomes loaded with NIN (MSCs-Lip@NCAF) to reverse PF in aged mice (Fig. 1). Specifically, MSCs-Lip@NCAF migrated to fibrotic lungs owing to the homing characteristics of MSCs, and matrix metalloproteinase–2 (MMP-2) overexpression in fibrotic lungs triggered the separation of Lip@NCAF and MSCs. Subsequently, Lip@NCAF decorated with type I collagenase and fibroblast activation protein (FAP) target peptide could degrade collagen fibers, improve drug delivery to fibroblasts, and further inhibit fibroblast overactivation and ECM synthesis. Furthermore, the differentiation of MSCs into AEC IIs

[1]State Key Laboratory of Natural Medicines, Department of Pharmaceutics, China Pharmaceutical University, Nanjing 210009, China. [2]Department of Endocrinology, Zhongda Hospital, School of Medicine, Southeast University, Nanjing 210009, China. [3]Jiangsu Key Laboratory of Druggability of Biopharmaceuticals, China Pharmaceutical University, Nanjing 210009, China. [4]Department of Precision Medicine, School of Medicine, Sungkyunkwan University, Suwon 16419, Republic of Korea. [5]College of Pharmacy, Yanbian University, Yanji 133002, China.
*Corresponding author. Email: jianghulin3@gmail.com, jianghulin3@163.com
†These authors contributed equally to this work.

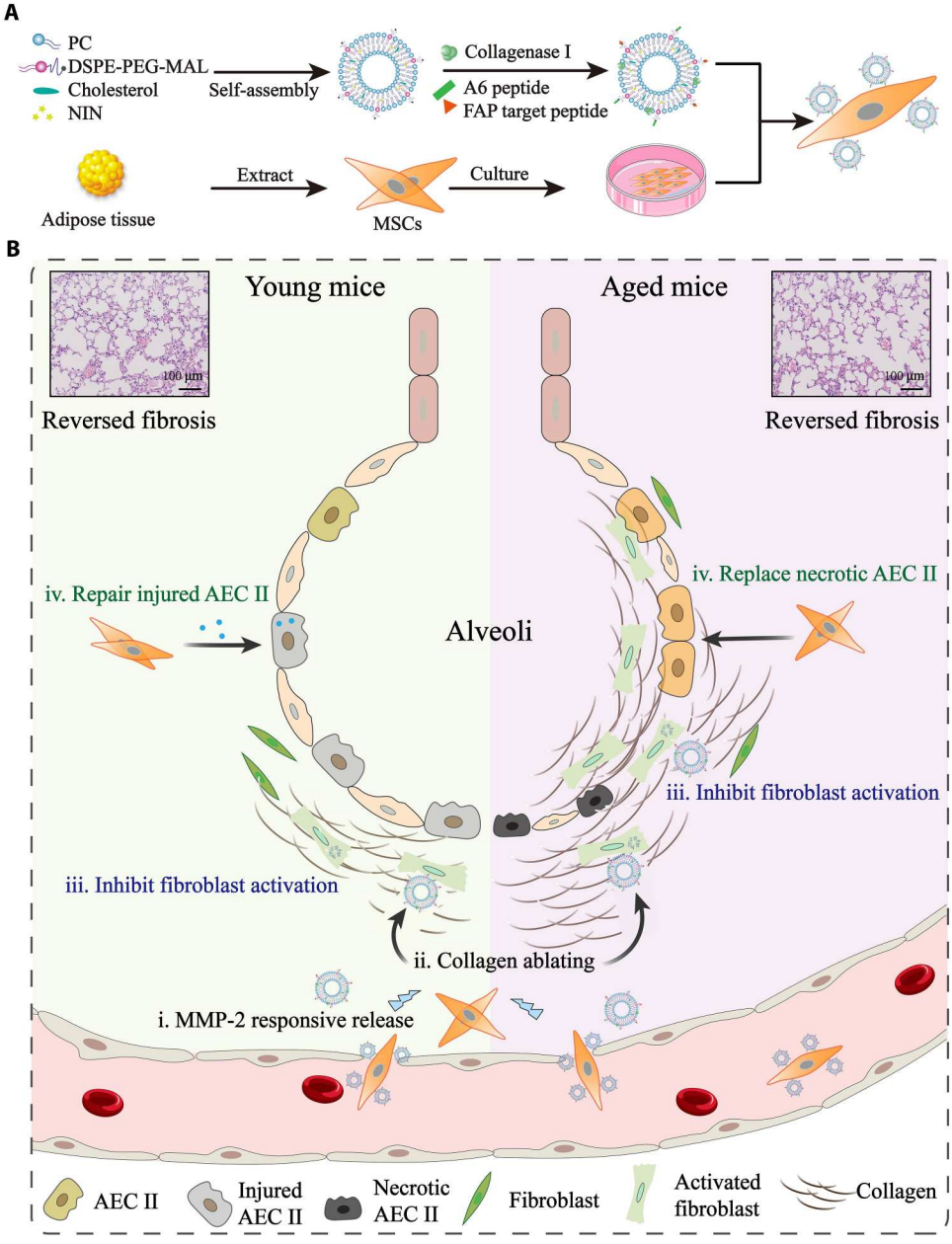

Fig. 1. Illustration of lung-targeting nanoengineered MSCs-Lip@NCAF designed to reverse PF in young and aged mice. (**A**) Preparation of MSCs-Lip@NCAF. PC, phosphatidylcholine. (**B**) MSCs-Lip@NCAF migrated to injured lungs because of their homing ability, and Lip@NCAF was released in response to MMP-2. Then, Lip@NCAF degraded collagen fibers and inhibited fibroblast overactivation. Moreover, MSCs repaired injured AEC IIs in young mice and differentiated into AEC IIs to participate in alveolar reestablishment in aged mice.

to participate in alveolar reestablishment in aged mice was also investigated.

RESULTS

PF progression in young and aged mice

It was reported that aged mice exhibited severe fibrosis after bleomycin (BLM) instillation, which highly recapitulates the pathological characteristics of human PF (*29*). To comprehensively study the progression of fibrosis at different ages, we intratracheally instilled young mice (2 months) and aged mice (16 months) with BLM (2 United States Pharmacopeia units/kg; Fig. 2A). The lungs of young mice exhibited inflammatory cell infiltration and thickened alveolar walls within 28 days and then recovered to normal levels after 28 days. However, a cracked alveolar structure was continuously observed in aged mice within 60 days (Fig. 2B and fig. S1A). Collagen I deposition was detected by immunofluorescence (IF) staining. As shown in Fig. 2C and fig. S1B, strong fluorescence was maintained at a steady state in young and aged mice for 28 days, but faint fluorescence was observed in young mice after 28

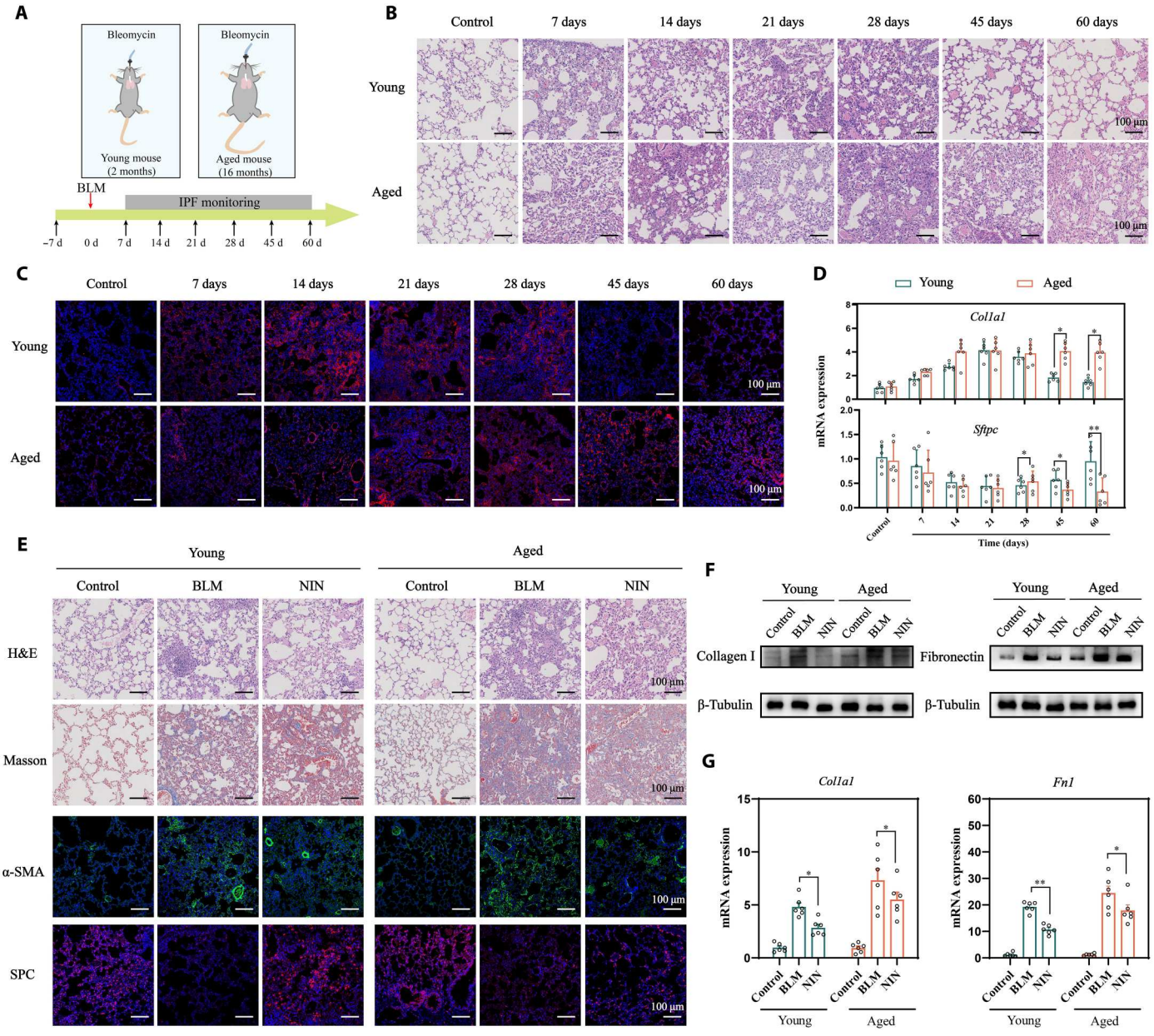

Fig. 2. PF progression in young and aged mice. (**A**) Schematic illustration of the study design. H&E staining (**B**) and IF staining of collagen I (**C**) in the lungs of young and aged mice challenged with BLM ($n = 6$). (**D**) RNA expressions of *Col1a1* and *Sftpc* in the lung of BLM-treated young and aged mice. (**E**) H&E, Masson, and IF staining of the lungs of young and aged mice treated with NIN ($n = 6$). WB (**F**) and qPCR (**G**) analysis of collagen I and fibronectin ($n = 6$). Data are means ± SEM. *$P < 0.05$ and **$P < 0.01$.

days. Quantitative polymerase chain reaction (qPCR) analysis further indicated that aged mice maintained augmented induction of *Col1a1* and decreased *Sftpc* expression after 28 days in contrast to young mice (Fig. 2D). These results showed that spontaneous reversal of fibrosis in young mice typically occurred 28 days after intratracheal BLM administration, while aged mice developed more severe fibrosis (*30*, *31*). To date, NIN has been approved to treat and delay the development of PF (*32*). After young and aged mice were challenged with BLM for 7 days, the mice received daily intragastric administration of NIN (60 mg/kg) for 14 days. As shown in Fig. 2E, hematoxylin and eosin (H&E) staining showed that the damage to alveoli and thickening of alveolar walls were significantly improved compared with those of BLM-treated young mice (fig. S1C). Decreased deposition of collagen fibers was observed by Masson staining. As indicated by the decrease in α–smooth muscle actin (α-SMA) and the increase in surfactant protein C (SPC) levels, NIN exerted considerable therapeutic effects on young mice. However, the lungs of aged mice featured a damaged alveolar structure, excessive collagen deposition, higher α-SMA levels, and lower SPC levels (fig. S1, D to F), which were further verified by Western blotting (WB) and qPCR (Fig. 2, F and G, and fig. S1, G and H). These results illustrated that NIN could decelerate the progression of fibrosis in young mice to some extent through inhibiting fibroblast activation and collagen synthesis. Nevertheless, the

therapeutic effect of NIN was limited in aged mice mainly because its low delivery efficiency to the lungs in the presence of compact collagen fibers, and the impotence of the repairment of injured AEC IIs.

Fabrication and characterization of MSCs-Lip@NCAF

Inspired by the excellent traits of MSCs, we constructed nanoengineered MSCs to treat PF in young and aged mice. MSCs were extracted from the adipose tissue of Sprague-Dawley rats using enzymatic digestion (*33*). The morphology of MSCs was fusiform (fig. S2). Flow cytometry (FCM) was used to verify the specific surface markers of MSCs. The results revealed that MSCs constitutively expressed high levels of CD29, CD44, and CD90 but not CD45, which was consistent with the literatures (fig. S3) (*25*, *34*). Next, Lip@N was prepared using the film dispersion method, and NIN was encapsulated within the lipid layer. Type I collagenase was inserted on the surface of Lip@N through hydrophobic interactions, and then the A6 peptide and FAP target peptide were grafted onto Lip@NC via Michael addition to obtain Lip@NCAF. The graft ratios of type I collagenase attached on Lip@NC and Lip@NCAF were 1.62 ± 0.46% and 1.53 ± 0.23%, respectively (fig. S4). Then, as determined by the ^{1}H nuclear magnetic resonance (^{1}H-NMR) spectrum and high-performance liquid chromatography (HPLC), the A6 peptide and FAP target peptide were successfully bound, and the graft ratios of Lip@NCAF were 1.32 ± 0.34% and 1.60 ± 0.14%, respectively (figs. S5 and S6). Lip@NCAF exhibited a particle size of 89.25 ± 0.43 nm, zeta potential of −2.76 ± 0.28 mV, encapsulation efficiency (EE) of 93.48 ± 0.28%, and loading capacity (LC) of 2.25 ± 0.68% (fig. S7 and table S1). The stability of Lip@NCAF was favorable in phosphate-buffered saline (PBS) (pH 7.4) and Dulbecco's modified Eagle's medium (DMEM) containing 10% fetal bovine serum (FBS) (fig. S8).

We established MSCs-Lip@NCAF via specific bioconjugation of the CD44 receptor and A6 peptide (fig. S9). The viability was greater than 80% after MSCs were incubated with different concentrations of Lip@NCAF for different times (fig. S10A). Moreover, the Lip@NCAF could specifically attach to the surface of MSCs without endocytosis within 8 hours (fig. S11). The reasons may be that A6 peptide conjugated on the surface of the Lip@NCAF is a long-chain peptide that limits internalization into the MSCs. MSCs-Lip@NCAF had the LC of 33.45 ± 0.42 pg per cell when MSCs were treated with Lip@NCAF at NIN concentration of 10 μM for 2 hours (fig. S10, B and C). The particle size of MSCs-Lip@NCAF increased to 5586.30 ± 7.15 nm in comparison to that of MSCs (4824.94 ± 5.97 nm), and the zeta potential of MSCs and MSCs-Lip@NCAF was negative (Fig. 3, A and B). Scanning electron microscopy was used to capture images of circular particles attached to the surface of MSCs (Fig. 3C). Moreover, 3,3′-dioctadecyloxacarbocyanine perchlorate–labeled Lip@CAF largely overlapped with 1,1′-Dioctadecyl-3,3,3′,3′-tetramethylindodicarbocyanine–labeled MSCs by confocal laser scanning microscopy (CLSM) (Fig. 3D). FCM further indicated the formation of MSCs-Lip@CAF and showed that DiD-labeled MSCs and DiO-labeled Lip@CAF were in the double-positive quadrant (Fig. 3E). These results indicated the efficient adhesion of Lip@NCAF to MSCs.

Next, the multidirectional differentiation potential of MSCs-Lip@NCAF was evaluated. Compared with MSCs, MSCs-Lip@NCAF showed similar calcium nodules and lipid droplets, demonstrating that Lip@NCAF did not affect the multidirectional differentiation potential of MSCs (Fig. 3F). Next, a Transwell model was used to assess the migration capacity of MSCs-Lip@NCAF. As shown in Fig. 3G, MSCs-Lip@NCAF responded to the C-X-C motif chemokine ligand 12 (CXCL12) in the lower chambers and migrated through the membrane, indicating that Lip@NCAF conjugation had negligible effects on the migration of MSCs. Then, MMP-2 was used to trigger Lip@NCAF release from MSCs. As shown in Fig. 3H, DiO-labeled Lip@CAF was dispersed in the periphery of DiD-labeled MSCs, indicating the separation of Lip@CAF and MSCs, which was further verified by FCM (Fig. 3I).

Antifibrotic effects of MSCs-Lip@NCAF in vitro

To study the antifibrotic effects of Lip@NCAF, we first extracted and identified fibroblasts from young and aged mice (y-fibroblasts and a-fibroblasts) (fig. S12). The viability was greater than 85% after these cells were incubated with different concentrations of Lip@NCAF (fig. S13). Collagen I was seeded on the Transwell insert, and different formulations labeled with coumarin 6 were added to the upper chambers. The uptake of the formulations by y-fibroblasts was evaluated by FCM (Fig. 4A). As shown in Fig. 4 (B to D), coumarin 6–labeled Lip@C and Lip@CAF showed increased fluorescence, suggesting that type I collagenase decoration could penetrate the collagen layer and improve the intracellular accumulation of Lip@NCAF. Likewise, similar results were observed in a-fibroblasts (fig. S14).

After Lip@NCAF was released, penetrated the collagen layer, and was internalized by fibroblasts, we investigated the inhibitory effects of Lip@NCAF on y-fibroblasts and a-fibroblasts. 5-Ethynyl-2′-deoxyuridine (EdU) can be incorporated into the DNA during cell proliferation and then labeled with Alexa Fluor 488 via click reaction (*35*). As shown in Fig. 4 (E and F), the fluorescence intensity was strongest after these cells were treated with transforming growth factor–β (TGF-β). An obvious decrease was observed after incubation with Lip@NCAF, suggesting the inhibition of fibroblast proliferation. The expression of collagen I and α-SMA was examined to evaluate the inhibition of fibroblast activation and collagen synthesis. In the presence of TGF-β, y-fibroblasts and a-fibroblasts exhibited strong red fluorescence. After treatment with different formulations, collagen I and α-SMA fluorescence decreased to varying degrees, and a faint fluorescence was detected in the cells treated with Lip@NCAF (Fig. 4G and fig. S15, A to D). Likewise, the protein expression of fibronectin and collagen I significantly decreased after the cells were treated with Lip@NCAF (Fig. 4, H and I, and fig. S15, E to H). Three-dimensional collagen gels were used to examine collagen contraction. When y-fibroblasts and a-fibroblasts were activated with TGF-β, the gel area was 27.76 ± 6.04% and 25.34 ± 4.68%, while the gel area increased to 89.68 ± 1.08% and 92.63 ± 3.36% after incubation with Lip@NCAF, suggesting that Lip@NCAF could impair fibroblast-mediated contraction of collagen fibers (Fig. 4, J and K). These data indicated that treatment with Lip@NCAF could decrease fibroblast hyperactivation, as indicated by the decreases in proliferation; expression of collagen I, α-SMA, and fibronectin; and collagen contraction.

It was reported that AEC IIs are exposed to continuous external stimuli and then release inflammatory factors, which is accompanied by epithelial-mesenchymal transition (EMT), leading to fibrosis exacerbation (*36*). Thus, we investigated the inhibitory effects of MSCs-Lip@NCAF on EMT by measuring vimentin. As shown in Fig. 4L, strong green fluorescence was observed when A549 cells

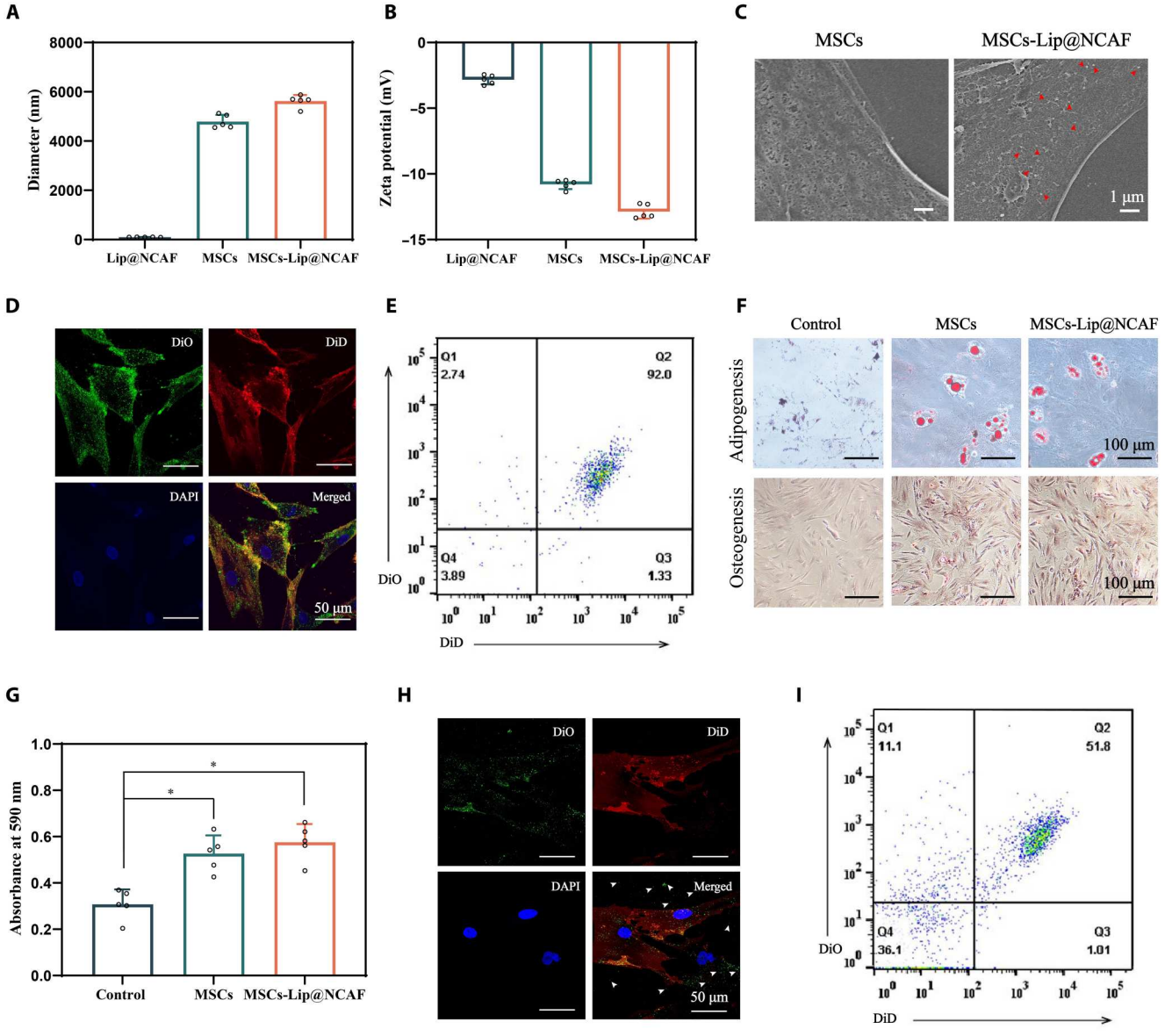

Fig. 3. Preparation and characterization of MSCs-Lip@NCAF. The size distribution (**A**) and zeta potential (**B**) of Lip@NCAF, MSCs, and MSCs-Lip@NCAF (n = 5). (**C**) Scanning electron microscopy images of MSCs and MSCs-Lip@NCAF. Fluorescence images of DiO-labeled Lip@CAF and DiD-labeled MSCs, as determined by CLSM (**D**) and FCM (**E**). (**F**) Adipogenic and osteogenic differentiation of MSCs and MSCs-Lip@NCAF. (**G**) The migration of MSCs and MSCs-Lip@NCAF in the presence of CXCL12 (n = 5). Fluorescence images of DiD-labeled MSCs and released DiO-labeled Lip@CAF in the presence of MMP-2, as determined by CLSM (**H**) and FCM (**I**). Data are means ± SD. *P < 0.05.

were treated with BLM. However, MSCs and MSCs-Lip@NCAF groups showed weaker fluorescence, which was ascribed to the inhibition of EMT by MSCs. Then, 3-(4,5-dimethyl-2-thiazolyl)-2,5-diphenyl tetrazolium bromide (MTT) and EdU assays were performed to estimate the survival and proliferation of A549 cells. The cell viability reached 71.96 ± 3.56% when A549 cells were treated with BLM, whereas cell viability increased to 83.41 ± 4.85% and 86.54 ± 2.43% in the presence of MSCs and MSCs-Lip@NCAF (Fig. 4M). Likewise, the fluorescence intensity was increased after the cells were treated with MSCs and MSCs-Lip@NCAF (Fig. 4N), indicating that MSCs-Lip@NCAF improved the survival and proliferation of A549 cells. Together, these data revealed that MSCs-Lip@NCAF exerted excellent antifibrotic effects in vitro.

Homing abilities and behavior of MSCs-Lip@NCAF in vivo

To investigate the lung-targeting properties of MSCs-Lip@NCAF in vivo, DiR was selected as a fluorescence probe to label Lip@CAF, MSCs, and MSCs-Lip@CAF. Figure 5 (A and B) showed that DiR signals in the lungs were slightly weak at all time points in the mice injected with free DiR or DiR-labeled Lip@CAF, indicating inferior lung-targeting efficiency. In contrast, the mice injected with MSCs and MSCs-Lip@CAF exhibited stronger fluorescent signals. Next, we quantitatively examined the fluorescence distribution in major

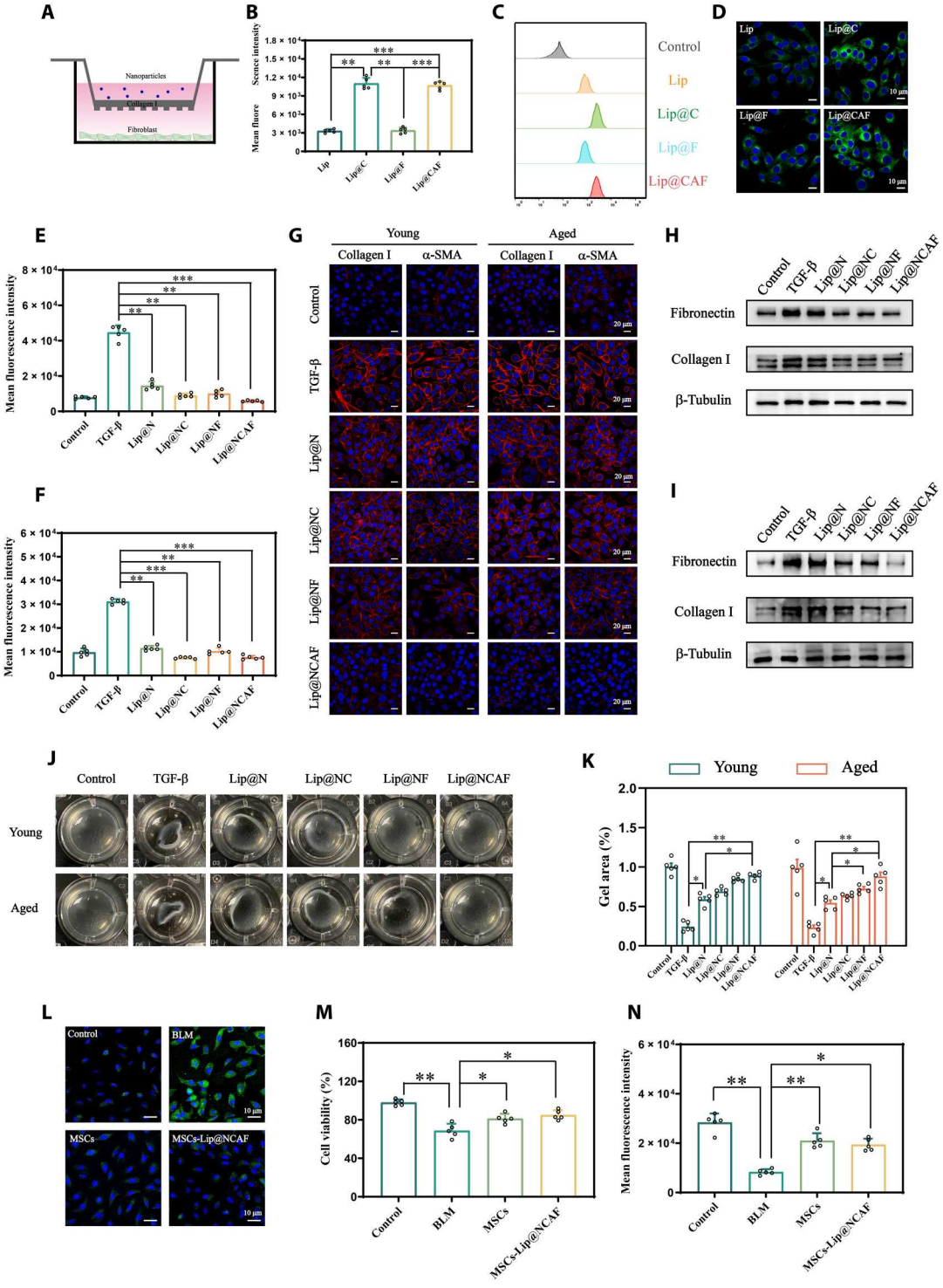

Fig. 4. The antifibrotic effects of MSCs-Lip@NCAF in vitro. (**A**) Illustration of the collagen barrier model in vitro. (**B** and **C**) The fluorescence intensity of y-fibroblasts was measured by FCM after adding different coumarin 6–labeled formulations to the Transwell chambers ($n = 5$). (**D**) Cellular uptake in y-fibroblasts, as shown by CLSM. Inhibition of y-fibroblast (**E**) and a-fibroblast (**F**) proliferation by Lip@NCAF, as shown by EdU staining ($n = 5$). (**G**) IF analysis of collagen I and α-SMA in y-fibroblasts and a-fibroblasts. WB analysis of fibronectin and collagen I in y-fibroblasts (**H**) and a-fibroblasts (**I**). (**J**) Images of collagen contraction mediated by y-fibroblasts and a-fibroblasts. (**K**) Quantitative analysis of the gel area in (J) ($n = 5$). (**L**) IF analysis of vimentin when A549 cells were incubated with MSCs and MSCs-Lip@NCAF in the presence of BLM. The survival (**M**) and proliferation (**N**) of A549 cells after incubation with MSCs and MSCs-Lip@NCAF in the presence of BLM ($n = 5$). Data are means ± SD. $^{*}P < 0.05$, $^{**}P < 0.01$, and $^{***}P < 0.001$.

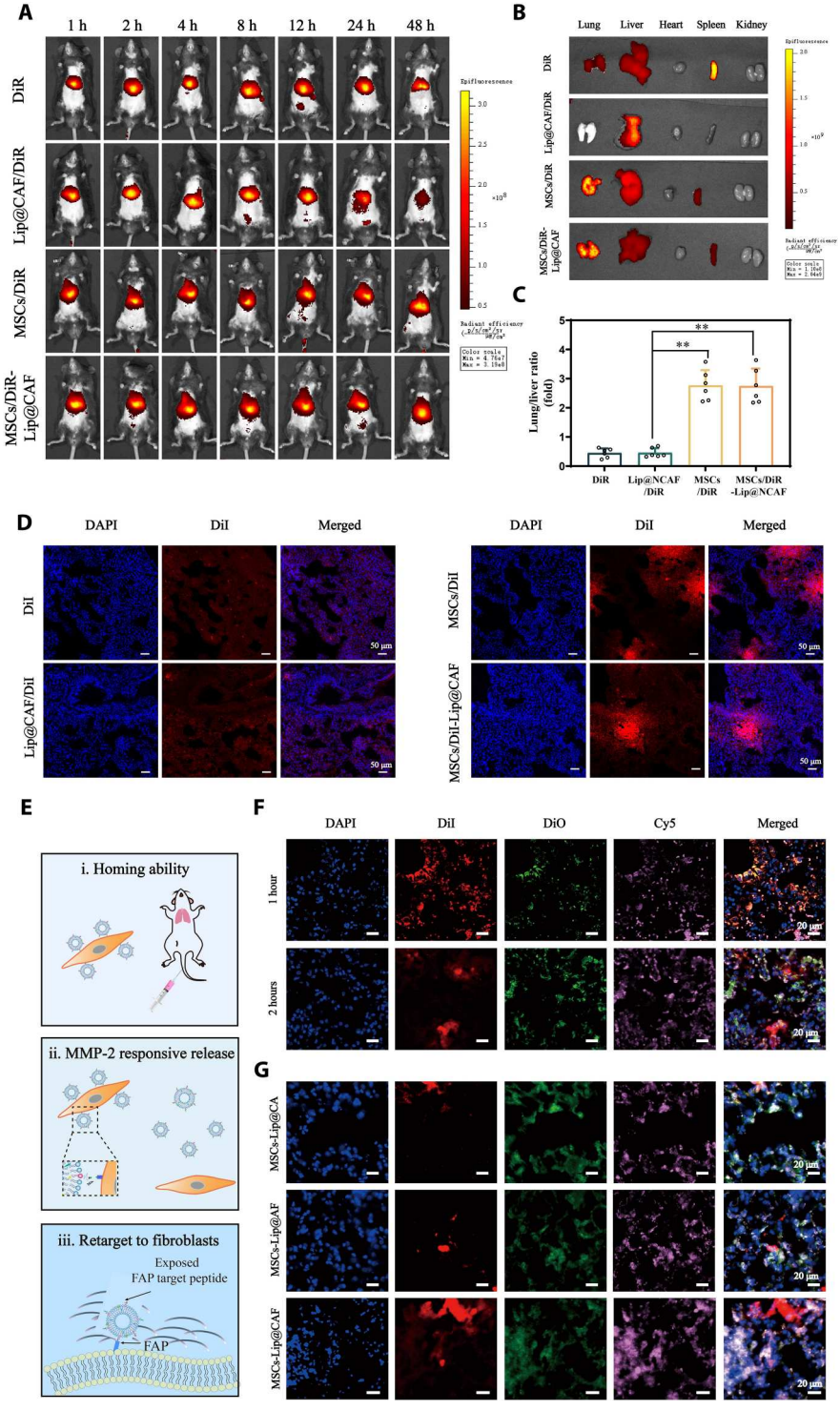

Fig. 5. Homing ability and behavior of MSCs-Lip@NCAF in vivo. (**A**) In vivo images of the mice that were intravenously injected with free DiR, DiR-labeled Lip@CAF, MSCs, and MSCs-Lip@CAF ($n = 6$). (**B**) Ex vivo images of major organs collected after 12 hours after injection ($n = 6$). (**C**) Quantification of the fluorescence intensity of lung/liver ($n = 6$). (**D**) Fluorescence imaging of lung sections after the injection of free DiI, DiI-labeled Lip@CAF, MSCs, and MSCs-Lip@CAF for 12 hours. (**E**) Illustration of the behavior of MSCs-Lip@NCAF in vivo. (**F**) Fluorescence imaging of the lungs of mice treated with double-labeled MSCs-Lip@CAF (MSCs labeled with DiI and Lip@CAF labeled with DiO) for 1 and 2 hours. (**G**) IF analysis of lung sections after mice were injected with MSCs-Lip@CA, MSCs-Lip@AF, and MSCs-Lip@CAF (DiO-labeled Lip@CA, Lip@AF, and Lip@CAF, as well as DiI-labeled MSCs) for 4 hours. Data are means ± SD. $^{**}P < 0.01$.

organs. The DiR fluorescence intensity of the lungs was 2.65- and 2.62-fold greater than that in the livers in the MSCs and MSCs-Lip@CAF groups, respectively (Fig. 5C). To further investigate the distribution of MSCs-Lip@NCAF in lungs, the mice treated with DiI-labeled formulations were euthanized, and the lungs were used to generate frozen sections. As shown in Fig. 5D, enhanced red fluorescence was observed specifically in the lungs of mice treated with MSCs and MSCs-Lip@CAF in comparison with those treated with free DiI and DiI-labeled Lip@CAF. Moreover, MSCs stably expressing green fluorescent protein (GFP) were used to further confirm the residence time of MSCs. As shown in fig. S16, obvious green fluorescence was observed specifically in the lungs of mice treated with MSCs-Lip@NCAF within 14 days. These data indicated that MSCs-Lip@NCAF could persistently accumulate in fibrotic lungs.

Next, we further investigated the behavior of MSCs-Lip@NCAF in vivo, including the homing capacity of MSCs-Lip@NCAF as well as the responsive release and the targeting capacity of Lip@NCAF (Fig. 5E). The mice with PF were intravenously injected with double-labeled MSCs-Lip@CAF (Lip@CAF labeled with DiO and MSCs labeled with DiI), and FAP-positive fibroblasts were labeled with cyanine5 (Cy5). One hour later, significant overlapping yellow fluorescence was observed within fibrotic lungs, revealing abundant accumulation of MSCs-Lip@CAF in the lungs. At 2 hours after injection, most of the green fluorescence was scattered in the periphery of the red fluorescence, suggesting the separation of Lip@CAF and MSCs (Fig. 5F and fig. S17A). Four hours after dosing, strong white fluorescence was observed when the mice were treated with MSCs-Lip@CAF compared with MSCs-Lip@CA and MSCs-Lip@AF (Fig. 5G). Colocalization coefficients of MSCs-Lip@CA and MSCs-Lip@AF were 0.40 ± 0.08 and 0.42 ± 0.10, while that of MSCs-Lip@CAF increased to 0.73 ± 0.11 (fig. S17B). This increased degree of colocalization between Lip@CAF and FAP suggested that Lip@CAF could efficiently degrade collagen fibers and target fibroblasts. Collectively, these results suggested that MSCs-Lip@NCAF had the native homing ability to fibrotic lungs and that Lip@NCAF could responsively release and target fibroblasts.

Antifibrotic effects of MSCs-Lip@NCAF on young mice

After confirming the effective delivery of MSCs-Lip@NCAF to fibrotic lungs, we evaluated the antifibrotic performance of MSCs-Lip@NCAF in vivo. BLM instillation for 7 days induced fibrogenesis (fig. S18). Seven days after BLM instillation, the mice were intravenously injected with normal saline, Lip@NCAF, MSCs, MSCs-Lip@NCA, MSCs-Lip@NAF, and MSCs-Lip@NCAF at a dose of 5×10^5 cells per mouse or 3 mg/kg of NIN twice a week for 3 weeks. Simultaneously, NIN (60 mg/kg) was intragastrically administrated as a positive drug group. As shown in Fig. 6A, the BLM group showed a continuous decrease in body weight, whereas varying increases were observed in mice treated with different formulations. Lung/body weight and hydroxyproline (HYP) were maintained at control-like levels in mice that were treated with MSCs-Lip@NCAF (Fig. 6, B and C). Obvious normalization of lung morphology was observed after treatment (Fig. 6D). We next conducted histological examinations of lung tissues. H&E staining revealed thickened alveolar walls and the infiltration of inflammatory cells in the BLM group. After treatment with MSCs-Lip@NCAF, infiltrated inflammatory foci and tissue density were close to those in the control group compared with MSCs (fig. S19A). Likewise, collagen fiber deposition decreased after treatment with different formulations, and MSCs-Lip@NCAF induced a marked decline (Fig. 6D). In addition, antifibrotic efficacy was further confirmed by measuring the expression of collagen I and α-SMA using immunohistochemical (IHC) techniques. Decreased expression of collagen I and α-SMA was observed in MSCs-Lip@NCAF–treated mice (Fig. 6D and fig. S19, B to D). Similar results were also verified by WB and qPCR, indicating the inhibition of fibroblast overactivation and collagen synthesis (Fig. 6, E to G, and fig. S19E). More decreased fibronectin and increased SPC levels were observed after treatment with MSCs-Lip@NCAF (Fig. 6, H to J, and fig. S19, F and G). The respiration parameters were detected to evaluate the pulmonary function. As shown in fig. S20, MSCs-Lip@NCAF significantly improved the pulmonary function of young mice.

Next, MSCs-Lip@NC, MSCs-Lip@NA, and MSCs-Lip@NF were set as controls to study the superiority of type I collagenase and the modification of peptide. As shown in fig. S21, compared with MSCs-Lip@N, MSCs-Lip@NC, and MSCs-Lip@NF, MSCs-Lip@NA showed better recovery ability in lung structures and lower levels of collagen fiber and α-SMA because A6 peptide incorporation made Lip@NA attach to the MSCs, thus accumulating in lung sites. MSCs-Lip@NCAF displayed better antifibrotic effects than MSCs-Lip@NA because type I collagenase and FAP target peptide could efficiently degrade collagen fibers and target fibroblasts. Hence, the CAF modification endowed MSCs-Lip@NCAF with the ability of antifibrotic effects.

We also conducted biochemical analyses of alanine aminotransferase (ALT) and serum aspartate aminotransferase (AST) to evaluate systemic hepatotoxicity. The levels of ALT and AST were elevated in mice that were orally administrated NIN, whereas the levels in the MSCs-Lip@NCAF group were close to those in the control group, indicating negligible hepatotoxicity (fig. S22). Moreover, to evaluate the biosafety of different formulations to major organs, H&E staining was performed, and no conspicuous histopathological alterations were observed in the heart, liver, spleen, or kidney after a 3-week treatment (fig. S23). Together, these results suggested that MSCs-Lip@NCAF markedly ameliorated pulmonary function in young mice after BLM-induced injury without systemic toxicity.

Antifibrotic effects of MSCs-Lip@NCAF on aged mice

We examined the curative effects of MSCs-Lip@NCAF against PF in aged mice. The dosing regimen was identical to that of young mice. As shown in Fig. 7A, H&E staining showed that the lungs exhibited distinctively thickened alveolar walls and observable distortions in lung structures after aged mice were treated with BLM. Treatment with NIN did not improve pulmonary damage owing to its low delivery efficiency to the lungs and the impotence of the repairment of injured AEC IIs. Ashcroft score was decreased in the MSCs-Lip@NCAF group (fig. S24A). Significant collagen fiber deposition was found in sections from the BLM, NIN, and Lip@NCAF groups. Nevertheless, MSCs down-regulated the levels of collagen fibers, and more significant decreases were observed in the MSCs-Lip@NCAF group, which was consistent with quantitative results (fig. S24B). Moreover, the expression of collagen I and α-SMA was elevated in BLM-treated mice; however, treatment with MSCs-Lip@NCAF down-regulated the levels of collagen I and α-SMA (fig. S24, C and D). The expression of SPC was enhanced when the mice were injected with MSCs-Lip@NCAF (fig. S24E).

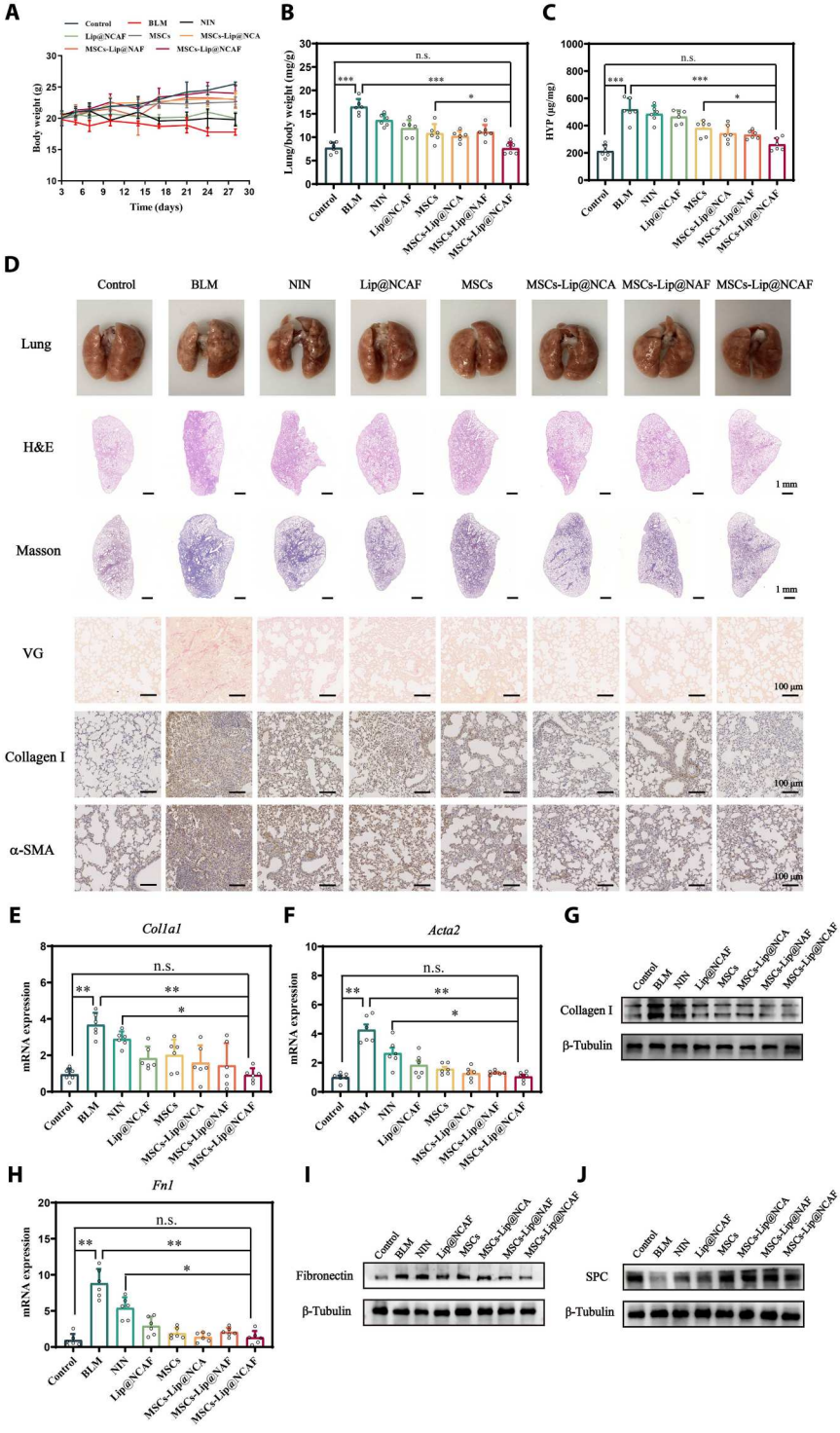

Fig. 6. Antifibrotic effects of MSCs-Lip@NCAF on young mice. (**A**) Body weight after treatment with different formulations ($n = 6$). (**B**) Lung/body weight in the different groups ($n = 6$). (**C**) The levels of HYP ($n = 6$). (**D**) Morphology and H&E, Masson, and IHC staining of lung sections. RNA levels of *Col1a1* (**E**) and *Acta2* (**F**) ($n = 6$). (**G**) WB analysis of collagen I. qPCR (**H**) and WB (**I**) of fibronectin ($n = 6$). (**J**) The expression of SPC was analyzed by WB. Data are means ± SD (A) to (C) or means ± SEM (E), (F), and (H). *$P < 0.05$, **$P < 0.01$, and ***$P < 0.001$. n.s., no significant difference.

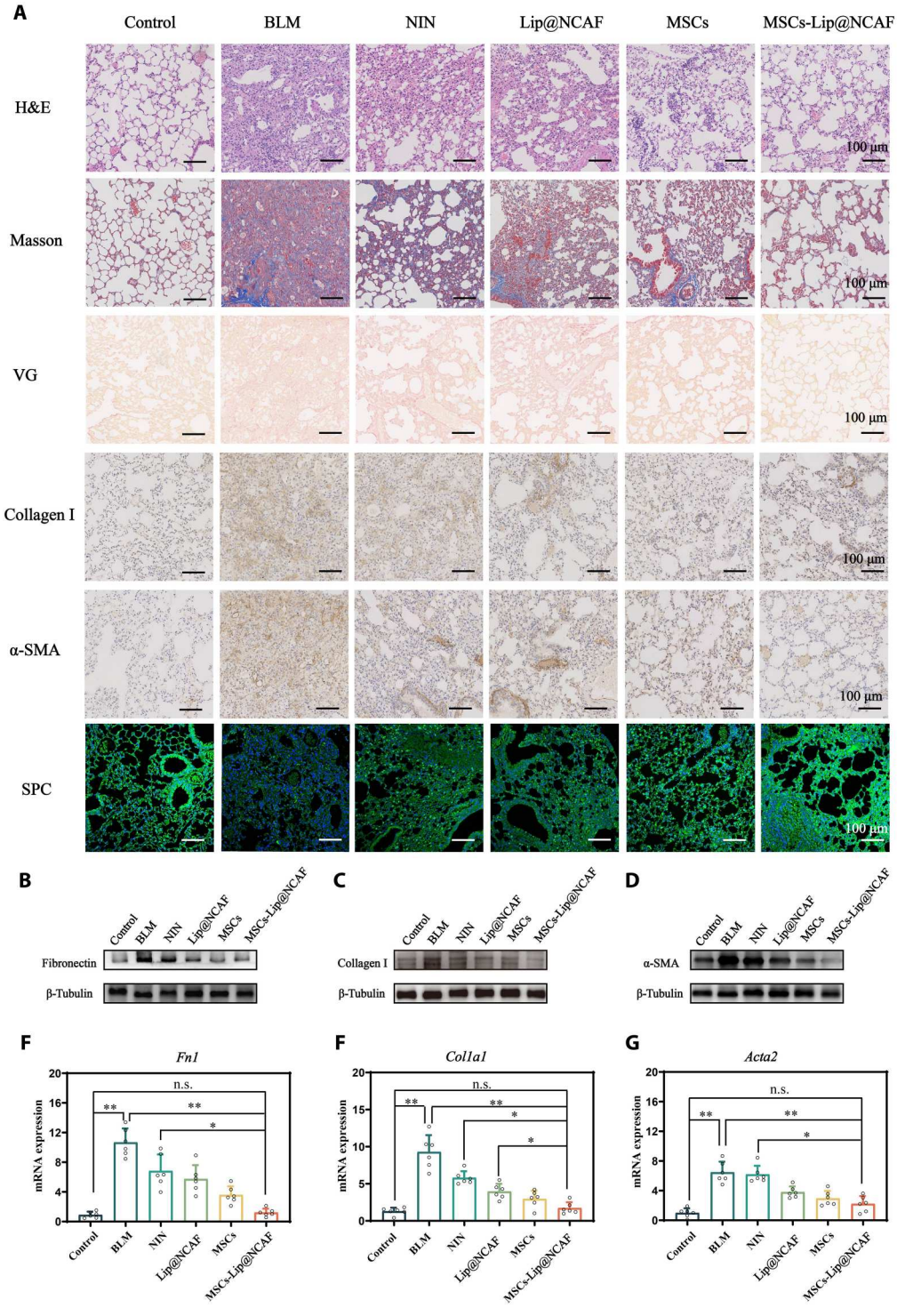

Fig. 7. Antifibrotic effects of MSCs-Lip@NCAF on aged mice. (**A**) H&E, Masson, IHC, and IF staining of lung sections from aged mice treated with different formulations ($n = 6$). The expressions of fibronectin (**B**), collagen I (**C**), and α-SMA (**D**) by WB ($n = 6$). RNA levels of *Fn1* (**E**), *Col1a1* (**F**), and *Acta2* (**G**) ($n = 6$). Data are means ± SEM. $^{*}P < 0.05$ and $^{**}P < 0.01$.

The protein expression of fibronectin, collagen I, and α-SMA was analyzed by WB. As shown in Fig. 7 (B to D), protein expression was obviously increased after BLM instillation, whereas it returned to normal levels in the MSCs-Lip@NCAF group (fig. S24, F to H). Similar results were verified by qPCR analysis (Fig. 7, E to G), indicating the inhibition of fibroblast overactivation and ECM deposition. The results suggested that MSCs-Lip@NCAF had superior therapeutic effects than MSCs alone because Lip@NCAF could penetrate collagen fibers, retarget fibroblasts, and inhibit fibroblast overactivation. Moreover, ALT and AST levels were elevated approximately twofold in mice that were orally administrated NIN compared to those in the control group, but MSCs-Lip@NCAF–treated mice exhibited normal levels of these enzymes (fig. S25). H&E staining was also performed to evaluate the biosafety of different formulations to major organs, and no obvious histopathological alterations were found in the heart, liver, spleen, or kidney (fig. S26). These results indicated that NIN exerted negligible effects against PF in aged mice, while intravenous injection of MSCs-Lip@NCAF alleviated severe fibrosis as indicated by decreases in collagen I, α-SMA, and fibronectin levels and by increase in SPC levels without toxicity.

Antifibrotic mechanisms of MSCs-Lip@NCAF

We examined the antifibrotic mechanisms of Lip@NCAF in fibroblasts (Fig. 8A). After fibroblasts were treated with platelet-derived growth factor–BB (PDGF-BB), phosphorylated PDGF receptor (p-PDGFR) and phosphorylated extracellular signal–regulated kinase 1/2 (p-ERK1/2) levels were increased, followed by an increase in the RNA expression of *Col1a1* and *Pdgfrb*. However, Lip@NCAF-treated fibroblasts exhibited lower protein levels of p-PDGFR and p-ERK1/2 and decreased RNA levels of *Col1a1* and *Pdgfrb*, indicating that Lip@NCAF inhibited fibroblast overactivation by blocking the PDGFR-ERK1/2 pathway (Fig. 8, B to D, and fig. S27, A and B). Moreover, we set the groups of liposomes without NIN (named as Lip@CAF) and MSCs tethered with liposomes without NIN (named as MSCs-Lip@CAF) to support the pharmacological action of NIN in vivo. As shown in fig. S28, α-SMA and collagen I maintained higher expression levels after instillation with BLM, whereas varying decreases were observed in mice treated with different formulations. Compared with Lip@CAF and MSCs-Lip@CAF, the expressions of α-SMA and collagen I significantly decreased when the PF mice were injected with Lip@NCAF and MSCs-Lip@NCAF, which was attributed to the pharmacological action of NIN.

Next, to study the antifibrotic mechanisms of MSCs in vivo, we examined the levels of inflammatory factors. Treatment with MSCs and MSCs-Lip@NCAF down-regulated the levels of tumor necrosis factor–α (TNF-α), interleukin-1β (IL-1β), and IL-6 in young and aged mice (Fig. 8, E to G). To further trace the fate of MSCs in vivo, aged mice with PF were administrated a single injection of MSCs or MSCs-Lip@NCAF expressing GFP. After 14 days, the lungs were collected and subjected for IF analysis. MSCs expressing green fluorescence emitted red fluorescence, indicating the presence of SPC (yellow fluorescence) (Fig. 8H and fig. S27C). To further justify that the MSCs-Lip@NCAF can regenerate into AEC II, we constructed a cell-specific expressed plasmid containing an SPC promoter, which is associated with the formation of epithelial cell, is highly active in the early stage of AEC II formation, and is reliable to drive GFP expression (*37*, *38*). As shown in fig. S29, the lungs presented obvious green fluorescence in the MSCs and MSCs-Lip@NCAF groups. These data suggested that the MSCs differentiated into AEC IIs to participate in alveolar reestablishment, which was critical for aged mice with PF.

There is a growing body of evidence suggesting that the expression levels of cell cycle regulators, including *Cdkn2a* and *Cdkn1a*, are up-regulated in fibroblasts and epithelial cells in fibrotic lungs, resulting in cell death and the generation of fibrotic factors [MMP-12, monocyte chemoattractant protein-1 (MCP1), and TGF-β] (*39*). The RNA levels of *Cdkn2a*, *Cdkn1a*, *Mmp12*, and *Mcp1* were elevated when aged mice were subjected to BLM instillation, and treatment with different formulations reduced these RNA expression levels (Fig. 8, I to L), which was beneficial to the survival of epithelial cells and the integrity of the alveolar structure.

DISCUSSION

PF is a progressive and irreversible lung disease with high mortality. Currently, two approved drugs (NIN and PFD) can slow the progression of fibrosis (*40*, *41*). Unfortunately, curing aged patients with severe fibrosis is not effective because of insufficient accumulation of these drugs and wide necrocytosis of AEC IIs in lung tissue (*42*). We designed and established a versatile nanoengineered platform (MSCs-Lip@NCAF) to solve these issues in aged mice by improving drug accumulation and replacing necrotic AEC IIs.

Specifically, antifibrotic effects were achieved on the basis of MSCs and Lip@NCAF. Studies have shown that MSCs and MOMCs are multipotent stem cells that can be recruited to injured lungs through the specific interactions of chemotactic factors with chemokine receptors and are conducive to lung tissue repair and regeneration (*39*). Compared to MOMCs, MSCs also have outstanding immunoregulatory functions in inflammatory disorders (*43*). Our study demonstrated that MSCs were guided to injured lungs and decreased the levels of inflammatory factors to normalize the hostile microenvironment (Fig. 8, E to G). MSCs, not MOMC, could differentiate into AEC IIs to reestablish alveolar structure, which was crucial for treating aged mice with PF (Fig. 8H). Considering excessive collagen fiber deposition in fibrotic lungs, type I collagenase–decorated Lip@NCAF was prepared to degrade collagen fibers, efficiently deliver NIN, and inhibit fibroblast hyperactivation, as indicated by decreases in proliferation; expression of collagen I, α-SMA, and fibronectin; and collagen contraction. In summary, we constructed a cell-nanoparticle co-delivery system (MSCs-Lip@NCAF) to exert antifibrotic effects via the differentiation of MSCs into AEC IIs and collagen-ablating functions to efficiently deliver Lip@NCAF.

In addition, MSCs-Lip@NCAF was strategically distinct from conventional drug-loaded cell carriers (*44*). Current methods for constructing cell carriers, such as by directly internalizing nanocarriers within cells, suffer from several drawbacks. A complex intracellular environment might degrade internalized nanocarriers, which influences the physiological characteristics of the cell carriers (*45*). Moreover, the MSCs were reprogrammed by injecting virus particles that have been manipulated to carry genetic information, which brought a potential security threat (*46*). Notably, Lip@NCAF adhered to the surface of the MSCs via specific biological ligand-receptor interactions in this study, which overcame these deficiencies. This cell-friendly modification was highly safe, reversed the fibrosis in young mice, and effectively treated the fibrosis of aged mice.

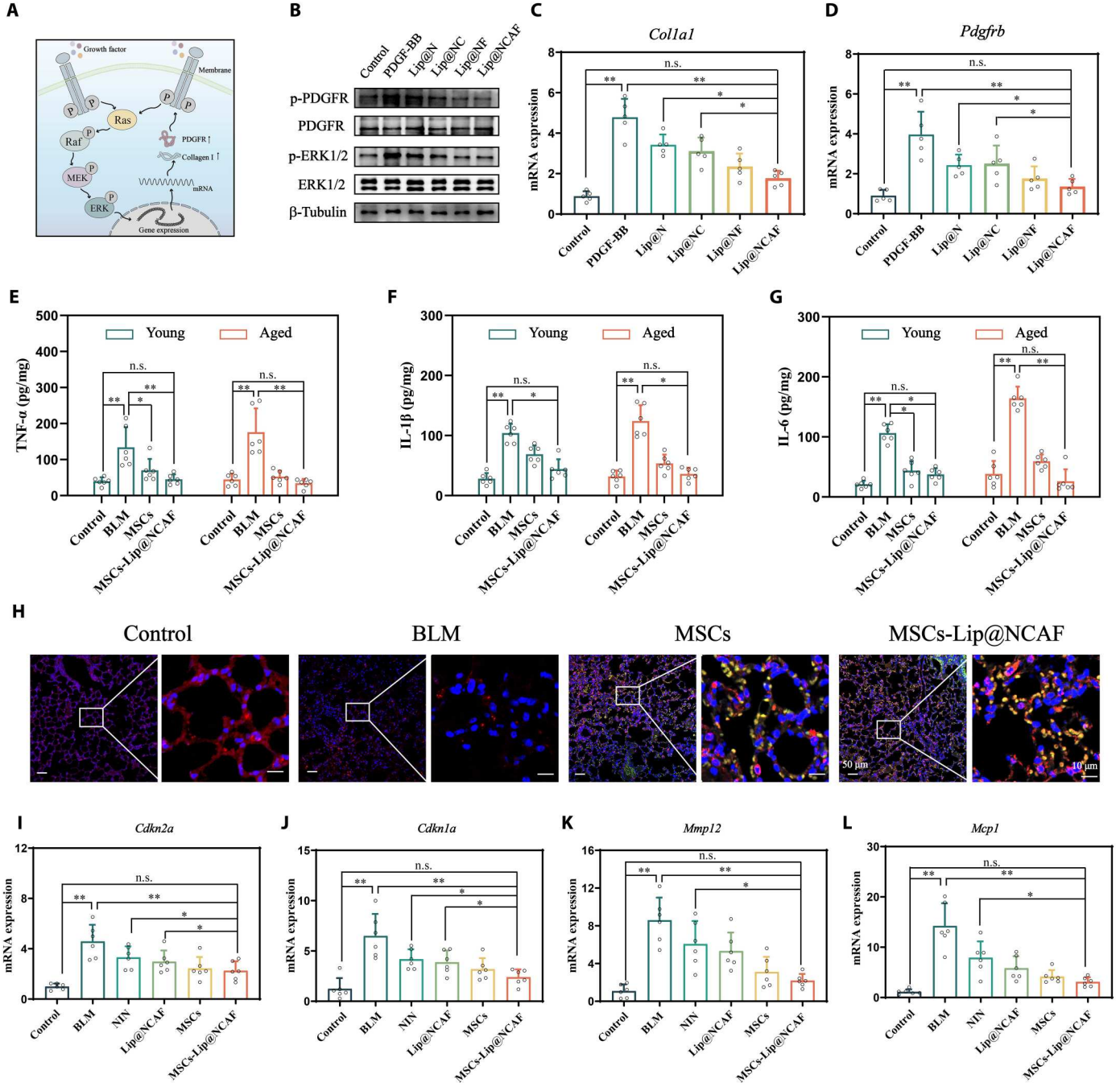

Fig. 8. Antifibrotic mechanisms of Lip@NCAF and MSCs. (**A**) Illustration of antifibrotic mechanisms of Lip@NCAF. MEK, mitogen-activated protein kinase kinase. (**B**) The expressions of p-PDGFR and p-ERK1/2 by WB. RNA levels of *Col1a1* (**C**) and *Pdgfrb* (**D**) ($n = 5$). The levels of TNF-α (**E**), IL-1β (**F**), and IL-6 (**G**) in young and aged mice treated with MSCs and MSCs-Lip@NCAF ($n = 6$). (**H**) IF analysis of the lung sections in aged mice injected with MSCs and MSCs-Lip@NCAF expressing GFP for 14 days ($n = 6$). RNA levels of *Cdkn2a* (**I**), *Cdkn1a* (**J**), *Mmp12* (**K**), and *Mcp1* (**L**) of lungs in aged mice ($n = 6$). Data are means ± SD (E) to (G) or means ± SEM (C), (D), and (I) to (L). *$P < 0.05$ and **$P < 0.01$.

Now, intratracheal instillation of BLM in young mice is the most widely used model to study the pathogenesis of PF and the efficacy of therapeutics (*31*). However, in young mice, fibrosis was spontaneously reversed 4 weeks after intratracheal BLM instillation (*30*). Therefore, the options for the administration time are quite short. When this limitation of the BLM model is not taken into consideration in the experimental design plan, the results can be misleading (*47*). However, aged mice developed worse and long-term fibrosis after BLM instillation, which is highly analogous to the age of onset of patients with PF in clinic and recapitulated the pathogenetic characteristics of human PF. In our study, aged mice were first used to investigate the efficacy of therapeutic strategies.

We found that aged mice exhibited distorted alveolar structures within 60 days, and NIN had negligible effects on aged mice (Fig. 2, B and E). MSCs-Lip@NCAF reversed PF in young mice and effectively treated PF in aged mice mainly through AEC II regeneration to remodel lung structure.

In conclusion, we constructed MSCs-Lip@NCAF, which is a versatile PF-curative platform by assembling MSCs and Lip@NCAF. MSCs-Lip@NCAF exhibited rapid lung targeting and persistent accumulation within fibrotic lungs. When MMP-2 was overexpressed in fibrotic lungs, Lip@NCAF was released from MSCs, and the exposed type I collagenase degraded collagen fibers and improved the intracellular accumulation of these nanoparticles. Furthermore, MSCs differentiated into AEC IIs to participate in reestablishing lung function. Specifically, MSCs and liposomes have been widely used in clinic, which indicates that MSCs-Lip@NCAF have certain advantages for further clinical development. Overall, our strategy of MSCs-Lip@NCAF provides inspiration for the design of PF therapies, especially for treating aged patients.

MATERIALS AND METHODS

Materials

Phospholipid was purchased from Avanti (Shanghai, China). Cholesterol was purchased from Sinopharm Chemical Reagent Co. Ltd. (Beijing, China). 1,2-distearoyl-sn-glycero-3-phosphoethanolamine-N-[maleimide (polyethylene glycol)-2000] (DSPE-PEG_{2000}-MAL) was purchased from Shanghai Yarebio Co. Ltd. (Shanghai, China). A6 peptide (KPSSPPEECGPLGIAGQC) and FAP target peptide (DRGETGPAC) were synthesized by GL Biochem Ltd. (Shanghai, China). NIN was purchased from Aladdin (Shanghai, China). Type I collagenase and MMP-2 were purchased from Sigma-Aldrich (St. Louis, USA). Rat tail type I collagen was from Corning (NY, USA). MSCs expressing GFP and CXCL12 were purchased from Cyagen Biosciences Inc. (Guangzhou, China). The HYP assay kit was purchased from Nanjing Jiancheng Bioengineering Institute (Nanjing, China). The total RNA isolation kit was purchased from Foregene Co. Ltd. (Chengdu, China). All-In-One 5X RT MasterMix was purchased from Applied Biological Materials (Nanjing, China). The 2 × S6 Universal SYBR qPCR Mix was from EnzyArtisan Biotech Co. Ltd. (Shanghai, China). BLM was purchased from Zhejiang Hisun Pharmaceutical Co. Ltd. (Hangzhou, China). TGF-β was purchased from PeproTech Inc. (NJ, USA). Anti-fibronectin, anti-vimentin, anti-FAP, anti-SPC, and anti-ERK1/2 antibodies were purchased from Abcam (Cambridge, UK). Anti–collagen I and anti–α-SMA antibodies were purchased from Proteintech (Wuhan, China). PDGF-BB was purchased from GenScript (Nanjing, China). Lipofectamine 3000 was from Invitrogen (CA, USA). Confocal dishes were purchased from NEST Biotechnology (Wuxi, China). The rest were commercially qualified reagents.

PF progression of young and aged mice

Young (2 months) and aged (16 months) C57BL/6 mice were administrated with intratracheal injection of BLM (2 USP/kg). The control group was similarly treated with normal saline. Specifically, lung tissues were collected at different time points and fixed with 4% paraformaldehyde. The lungs were serially sectioned at 5 μm in thickness for H&E staining and IF analysis of collagen I. Then, RNA expressions of *Col1a1* and *Sftpc* were evaluated by qPCR. Briefly, 20 mg of lung tissue was homogenized to extract total RNA referring to the RNA isolation kit. Complementary DNA was obtained using the reverse transcription system, followed by qPCR analysis (FQD-96A, BIOER, China). The primers sequences are listed as table S2.

Next, NIN was applied to treat PF in young and aged mice. After instillation with BLM for 7 days, the mice were intragastrically administrated with NIN (60 mg/kg) once a day. After treatment for 14 days, the lung tissues were subjected for H&E staining, Masson staining, and IF staining of α-SMA and SPC. The expressions of collagen I and fibronectin were examined by WB. Briefly, the total protein was extracted from lung tissues. Thirty micrograms of protein was separated by gel electrophoresis and then transferred to nitrocellulose (NC) membrane by electroblotting (Tanon EPS300, China). Five percent skim milk dissolved in Tris buffered saline with Tween 20 was used to block nonspecific binding site. Anti–collagen I and anti-fibronectin rabbit antibodies were incubated with NC membrane at 4°C overnight and subsequently marked with horseradish peroxidase–conjugated goat anti-rabbit antibody for 2 hours at room temperature. After rinsing thrice, the NC membrane was imaged using a charge-coupled device image system (Tanon 4200, China). The antibody catalog number and dilution are listed as table S3. In addition, RNA expressions of *Col1a1* and *Fn1* were detected by qPCR analysis as the above procedure. Assay kits′ catalog numbers are listed as table S4.

Isolation and identification of MSCs

MSCs were isolated from the epididymal adipose tissue by enzymatic digestion. Briefly, adipose tissue was collected from Sprague-Dawley rats, cut into small pieces, and digested by type I collagenase. FBS was used to neutralize enzymatic digestion. The cells were cultured in DMEM with 10% FBS. After the 3-day culture, the cell medium was updated to remove unadhered impure cells. When 90% confluence was achieved, the cells were subcultured. Following passage, expression levels of CD29, CD44, CD45, and CD90 were analyzed by FCM (BD FACSCelesta, USA).

Preparation and characterization of Lip@NCAF

Phospholipid, cholesterol, DSPE-PEG_{2000}-MAL, and NIN were dissolved in 5 ml of dichloromethane at the mass ratio of 30:5:5:1. The solvent was evaporated at 37°C using a rotary evaporator. The lipid film was then rehydrated in 5 ml of PBS. The suspension was sonicated using a cell cracker (XO-1000D, ATPIO, China) for 3 min. Lip@N was obtained after ultrafiltration centrifugation (100 kDa; Millipore, USA). Type I collagenase was added and stirred at 4°C for 12 hours to obtain Lip@NC. The A6 peptide and FAP target peptide were finally added and incubated at 4°C for 12 hours. Lip@NCAF was obtained after ultracentrifugation. FAP target peptide was incubated with Lip@N overnight to prepare Lip@NF.

To quantify the amount of type I collagenase attached on Lip@NC and Lip@NCAF, 20 μl of fluorescein isothiocyanate–collagen I was incubated with Lip@NC and Lip@NCAF at 37°C for 2 hours. Then, the suspension was centrifuged at 10,000 rpm for 30 min. The fluorescence intensity of the supernatant was measured (excitation: 485 nm, emission: 530 nm) using a microplate reader (ID5, Molecular Devices, USA). The graft ratio of type I collagenase was calculated according to Eq. 1. ^{1}H-NMR spectra and HPLC were used to identify the A6 peptide and FAP target peptide attached on

Lip@NCAF. The graft ratios of A6 peptide or FAP target peptide were calculated according to Eq. 2.

Then, the size distribution and zeta potential were determined by Zetasizer Nano (ZS90, Malvern, UK). The micromorphology of various nanoparticles was observed under transmission electron microscope (H-7650, Hitachi, Japan). EE and LC of NIN were determined as follows: Ultrafiltration centrifugation was used to remove free NIN. After demulsification with methyl alcohol, the amount of NIN entrapped in nanoparticles and the total amount of NIN were detected by the ultraviolet spectrum. EE and LC were calculated referring to Eqs. 3 and 4.

$$\text{Graft ratio of type I collagenase } (\%) = \frac{W_{\text{type I collagenase grafted to Lip@NCAF}}}{W_{\text{Lip@NCAF}}} \times 100\% \quad (1)$$

$$\text{Graft ratio of A6 or FAP } (\%) = \frac{W_{\text{added A6 or FAP}} - W_{\text{free A6 or FAP}}}{W_{\text{Lip@NCAF}}} \times 100\% \quad (2)$$

$$\text{EE } (\%) = \frac{W_{\text{entrapped NIN}}}{W_{\text{total NIN}}} \times 100\% \quad (3)$$

$$\text{LC } (\%) = \frac{W_{\text{entrapped NIN}}}{W_{\text{materials and NIN}}} \times 100\% \quad (4)$$

In addition, PBS and DMEM containing 10% FBS were used to investigate the stability of various nanoparticles. Briefly, four nanoparticles were suspended in PBS and DMEM. The particle sizes were measured and recorded at predetermined time points.

Fabrication and characterization of MSCs-Lip@NCAF

MSCs-Lip@NCAF was prepared by incubating MSCs with Lip@NCAF. Briefly, the MSCs were seeded into a petri dish with a diameter of 10 cm at the density of 5×10^5 per dish. Lip@NCAF with a NIN concentration of 10 μM was added into MSCs medium and incubated for 1, 2, 4, and 8 hours at 37°C. These cells were collected and centrifuged at 1000 rpm for 5 min to remove uncombined Lip@NCAF. A6 peptide was preincubated with MSCs for 2 hours to saturate the CD44 receptors of MSCs to further confirm the combination mechanism. The bioconjugation of DiO-labeled Lip@NCAF and DiD-labeled MSCs was observed under CLSM (LSM700, Zeiss, Germany). Then, MTT assay was conducted to estimate the cytotoxicity of Lip@NCAF on MSCs. MSCs were cultured in 96-well plates at a density of 1×10^4 cells per well. After a 24-hour culture, Lip@NCAF diluted with FBS-free DMEM was added at different NIN concentrations and continued to culture. Optical density (OD) values at 490 nm were detected to calculate the viability of MSCs. Then, HPLC was used to examine the LC of MSCs to optimize the incubation conditions of MSCs and Lip@NCAF.

Next, the size distribution and zeta potential of MSCs-Lip@NCAF were measured. The distribution of Lip@NCAF on the surface of MSCs was observed under a scanning electron microscope (SU8010, Hitachi, Japan). Moreover, the bioconjugation of MSCs and Lip@NCAF was further confirmed by CLSM and FCM. Briefly, MSCs were cultured at a density of 1×10^5 cells per well and incubated until 90% confluence was achieved. The DiD-labeled MSCs were incubated with DiO-labeled Lip@CAF for 2 hours before analysis.

Multidirectional differentiation of MSCs-Lip@NCAF

For determining the multidirectional differentiation potential of MSCs-Lip@NCAF, osteogenic and lipogenic inducing conditional media were applied to make it easier to differentiate into osteoblasts and adipose cells. After a 21-day induction, Alizarin Red S and Oil Red O staining were used to evaluate osteogenic and lipogenic differentiation.

Migration property of MSCs-Lip@NCAF in vitro

The migration of MSCs-Lip@NCAF was studied using Transwell with pore sizes of 8.0 μm. MSCs or MSCs-Lip@NCAF were cultured into the upper chambers and incubated for 24 hours. CXCL12 was added into lower chambers at the concentration of 100 ng/ml and incubated for 24 hours. Last, the upper chambers were stained with 0.1% crystal violet, and OD values at 590 nm were detected after the cells were destained with 33% acetic acid.

Release of Lip@NCAF from MSCs-Lip@NCAF

MMP-2 was used to study the responsive release of Lip@NCAF from MSCs. Briefly, DiO-labeled Lip@CAF was incubated with DiD-labeled MSCs for 2 hours. MMP-2 (1 μg/ml) was added and cocultured for 1 hour. Then, MSCs and released Lip@CAF were detected by CLSM and FCM.

Cells

Young and aged mice received intratracheal instillation of BLM (2 USP/kg) for 14 days and were euthanized. The lungs were gathered and cut into small pieces (1 mm^3). Type I collagenase (1 mg/ml) and trypsin (0.125%) were added, and the tissues were digested at 37°C for 30 min, followed by centrifugation at 2000 rpm for 10 min. Small pieces were spread on the bottle of petri dish. The dish was reversely placed for 4 hours and then the medium was added. Fibroblasts climbed out from the margin of small tissue on day 3. The fibroblasts were subcultured when the density reached 80%. Fibroblasts from young and aged mice were named as y-fibroblasts and a-fibroblasts, respectively. Then, TGF-β was used to stimulate y-fibroblasts and a-fibroblasts for 24 hours to identify the phenotype of these cells; then, we detected the expression of α-SMA specifically expressed proteins by activated fibroblasts. A549 cells were from the American Type Culture Collection and maintained in DMEM containing 10% FBS, penicillin (100 U/ml), and streptomycin (100 μg/ml) at 37°C under 5% CO_2 environment.

Collagen penetration capacity of Lip@NCAF

Fifty microliters of rat tail type I collagen (1 mg/ml) was uniformly added on the polycarbonate membranes of Transwell chambers. After solidification at 37°C for 4 hours to form the collagen layer, y-fibroblasts or a-fibroblasts were cultured in 24-well plates at a density of 4×10^4 cells per well. After the 24-hour incubation, the medium in the lower chambers was replaced with 600 μl of medium. Coumarin 6–labeled blank Lip, Lip@C, Lip@F, and Lip@CAF were prepared as the above procedure and added into the upper

chambers. The cells were incubated at 37°C for 2 hours and detected by FCM and CLSM.

Inhibition of fibroblast proliferation by Lip@NCAF

EdU assay was applied to evaluate inhibitory effects of Lip@NCAF on fibroblast proliferation. Y-fibroblasts or a-fibroblasts were cultured in six-well plates at a density of 1×10^5 cells per well and incubated for 24 hours. TGF-β was added at the concentration of 10 ng/ml for 24 hours to activate fibroblasts. After treatment with Lip@N, Lip@NC, Lip@NF, and Lip@NCAF at NIN concentration of 10 μM for 24 hours, EdU solution was added and cocultured for 2 hours, followed by labeling with Alexa Fluor 488 via click reaction. The fluorescence intensity was detected by FCM.

Inhibition of collagen I and α-SMA expressions by Lip@NCAF

IF and WB were used to investigate inhibitory effects of Lip@NCAF on collagen I and α-SMA expressions in y-fibroblasts and a-fibroblasts. For IF analysis, y-fibroblasts and a-fibroblasts were seeded into confocal dishes at a density of 1×10^5 cells per well at the presence of TGF-β and incubated for 24 hours. Then, Lip@N, Lip@NC, Lip@NF, and Lip@NCAF were added at a NIN concentration of 10 μM for 24 hours. After washing thrice, the cells were immobilized by 4% paraformaldehyde and subsequently hyalinized using 0.2% Triton X-100. After blocking with 5% donkey serum for 30 min, the cells were incubated with anti–collagen I and anti–α-SMA rabbit antibodies overnight, followed by incubation with Alexa Fluor 647 goat anti-rabbit immunoglobulin G for 2 hours. The cells were finally counterstained with 4′,6-diamidino-2-phenylindole (DAPI) and observed under CLSM. The process of WB was similar with the "PF progression of young and aged mice" section.

Three-dimensional collagen gels

Rat tail type I collagen was neutralized with NaOH and mixed with y-fibroblasts or a-fibroblasts (volume ratio = 1:2). The mixture was cultured in 24-well plates at a density of 1×10^5 cells per well and coagulated for 1 hour at 37°C. The gels were photographed after treatment with different formulations for 48 hours, and the gel area was quantified using ImageJ software (MD, USA).

Inhibition of EMT by MSCs-Lip@NCAF

The cell slide was gently placed into 24-well plates. Then, A549 cells were seeded onto the slide and cultured for 24 hours in the presence of 100 nM BLM. MSCs or MSCs-Lip@NCAF were added into the upper chambers. After treatment for 24 hours, IF analysis of vimentin was conducted as the above procedure before CLSM imaging.

Improvement of survival and proliferation of A549 cells

A549 cells were seeded into 24-well plates at a density of 1×10^5 cells per well and cultured for 24 hours in the presence of BLM (100 nM). MSCs or MSCs-Lip@NCAF were seeded into a Transwell insert at a density of 1×10^4. After treatment for 24 hours, MTT and EdU assays were performed to estimate the survival and proliferation of A549 cells.

Animals

Male C57BL/6 mice (2 and 16 months) and Sprague-Dawley rats were obtained from Vital River Laboratory Animal Technology Co. Ltd. (Beijing, China). The animals were fed with water and laboratory rodent food under a pathogen-free animal condition. All animal experiments were performed according to the guiding principles of the Animal Experimentation Ethics Committee of China Pharmaceutical University (2022–05-002).

Imaging of lung-targeting property

DiR-labeled Lip@CAF, MSCs, and MSCs-Lip@CAF were prepared with the same procedure and normalized to the same levels. C57BL/6 mice (2 months) were instilled with BLM for 7 days to establish the PF model. The mice were intravenously injected with free DiR, DiR-labeled Lip@CAF, MSCs, and MSCs-Lip@CAF. Photographs were taken after 1, 2, 4, 8, 12, 24, and 48 hours after injection by PerkinElmer IVIS Lumina III (MA, USA). The major organs were dissected and subjected for ex vivo imaging. Fluorescence intensity of DiR was quantified by Living Image analysis software. To further observe MSCs-Lip@NCAF distribution in PF mice, the mice were injected with DiI-labeled formulations, and the lungs were collected after 12 hours after injection and fixed in 4% paraformaldehyde. The sections were counterstained with DAPI before observation under CLSM. Furthermore, MSCs stably expressing GFP were used to confirm the residence time of MSCs-Lip@NCAF. Specifically, the mice were injected with MSCs-Lip@NCAF for 1, 3, 5, 7, and 14 days. The lungs were performed paraffin section and observed under CLSM.

Behavior of MSCs-Lip@NCAF in vivo

To investigate the homing characteristic of MSCs-Lip@NCAF as well as the responsive release and target capacity of Lip@NCAF, the PF mice were injected with double-labeled MSCs-Lip@CAF (Lip@CAF labeled with DiO and MSCs labeled with DiI). FAP-positive fibroblasts were labeled by Cy5. After 1 and 2 hours after injection, the lungs were collected, followed by frozen sections. The sections were stained with DAPI before CLSM observation. Meanwhile, we prepared DiO-labeled Lip@CA, Lip@AF, and Lip@CAF to adhere the surface of MSCs to study the retarget capacity of released Lip@CAF. The lungs were gathered after 4 hours after injection. Frozen sections were stained by anti-FAP antibody and observed under CLSM.

Antifibrotic effects of MSCs-Lip@NCAF on young mice

C57BL/6 mice (2 months) received intratracheal injection of BLM (2 USP/kg) for 7 days to establish the PF model. The mice injected with normal saline served as a control. Lip@NCAF, MSCs, MSCs-Lip@NCA, MSCs-Lip@NAF, and MSCs-Lip@NCAF were prepared as the above procedure. The mice received intravenous injection at a dosage of 5×10^5 cells per mouse or 3 mg/kg of NIN twice a week for 3 weeks, and NIN (60 mg/kg) was intragastrically administrated as a positive drug group (*48*–*50*). Simultaneously, we set MSCs-Lip@NC (MSCs tethered liposomes modified with collagenase I), MSCs-Lip@NA (MSCs tethered liposomes modified with A6 peptide), and MSCs-Lip@NF (MSCs tethered liposomes modified with FAP target peptide) to study the superiority of type I collagenase and the modification of peptides.

During treatment with different formulations, the weight of these mice was recorded. Then, the lungs were photographed to observe morphologies and were weighted for calculating the lung/body weight ratio. The content of HYP in fibrotic lungs was determined, referring to HYP assay kit. Briefly, 30 mg of lung tissue was dissolved in 1 ml of hydrolysate in boiling water for 20 min, and the

hydrolysate was adjusted to pH 6.0 to 6.8. Then, activated carbon was added to decolorize the hydrolysate. The samples were detected at 550 nm after centrifugation at 3000 rpm for 20 min.

Furthermore, the lungs were investigated by H&E staining, Masson staining, and VanGieson (VG) staining. The protein expressions of collagen I, α-SMA, fibronectin, and SPC were evaluated using IHC or/and WB. We also detected RNA expressions of *Col1a1*, *Acta2*, and *Fn1*. Respiration indexes, including tidal volume, minute volume, and peak expiration flux, were measured by Buxco FinePointe Whole Body Plethysmography (NC, USA). Moreover, the contents of ALT and AST in serum were detected and the major organs were gathered and analyzed with H&E staining to evaluate the biosafety of different formulations.

Antifibrotic effects of MSCs-Lip@NCAF on aged mice

C57BL/6 mice (16 months) were intratracheally instilled with BLM (2 USP/kg) to establish the PF model. The mice were treated with Lip@NCAF, MSCs, and MSCs-Lip@NCAF as the above dosing regimen. Meanwhile, the mice injected with normal saline served as a control, and NIN (60 mg/kg) was intragastrically administrated as a positive drug group. After 3 weeks, the lungs were analyzed using H&E staining, Masson staining, and VG staining, followed by IHC of collagen I and α-SMA as well as IF of SPC. The protein expressions of fibronectin, collagen I, and α-SMA were investigated by WB. qPCR was used to detect RNA expressions of *Fn1*, *Col1a1*, *Acta2*, *Cdkn2a*, *Cdkn1a*, *Mmp12*, and *Mcp1*. In addition, the levels of ALT and AST in serum were detected, and the major organs were analyzed with H&E staining to evaluate the biosafety.

Antifibrotic mechanisms of NIN

Y-fibroblasts were cultured in six-well plates, and PDGF-BB (100 ng/ml) was used to phosphorylate PDGFR. After culture for 24 hours, the cells were incubated with Lip@N, Lip@NC, Lip@NF, and Lip@NCAF at a NIN concentration of 10 μM, followed by 24-hour incubation. The protein was extracted for examining the expressions of p-PDGFR and p-ERK1/2. Total RNA was extracted for detecting the expressions of *Col1a1* and *Pdgfrb*.

To study the antifibrotic mechanisms of NIN in vivo, the young mice with PF were treated with Lip@CAF, Lip@NCAF, MSCs-Lip@CAF, and MSCs-Lip@NCAF as the above dosing regimen. The expressions of α-SMA and collagen I were detected by IHC techniques.

Immunoregulation of MSCs-Lip@NCAF on young and aged mice

The levels of TNF-α, IL-1β, and IL-6 were determined, referring to the instruction of the enzyme-linked immunosorbent assay kit. The lungs were collected from young and aged mice and washed with cold normal saline, followed by tissue homogenate and centrifugation at 4°C and 5000 rpm for 1 hour. The levels of TNF-α, IL-1β, and IL-6 were calculated referring to the standard protocol.

Differentiation of MSCs-Lip@NCAF in vivo

MSCs that stably expressed GFP were applied to trace the fate of MSCs in vivo. Aged mice were challenged by BLM for 7 days and then intravenously injected MSCs and MSCs-Lip@NCAF expressing GFP. After treatment for 14 days, the mice were euthanized, then the lungs were collected, followed by IF staining of SPC before subject to observation under CLSM. Furthermore, to further verify the regeneration of MSCs into AEC IIs, we designed a cell-specific expressed plasmid containing a SPC promoter and GFP reporter gene. The plasmid was encapsulated into Lipofectamine 3000, and the MSCs were transfected for 24 hours. The transfected MSCs were collected and injected into aged mice for 7 days, followed by observation under CLSM.

Statistical analysis

Experiments were conducted in triplicate, and all data are presented as means ± SD or means ± SEM. GraphPad (version 9.0) was applied for graphing and one-way analysis of variance (ANOVA) to detect the significant differences between multiple groups. $P > 0.05$ represented no significant difference (n.s.), $^{*}P < 0.05$ represented significant difference, and $^{**}P < 0.01$ and $^{***}P < 0.001$ represented highly significant difference. ImageJ software was applied for quantitative analysis.

Supplementary Materials

This PDF file includes:

Figs. S1 to S29

Tables S1 to S4

View/request a protocol for this paper from *Bio-protocol*.

REFERENCES AND NOTES

1. R. K. Albert, D. A. Schwartz, Revealing the secrets of idiopathic pulmonary fibrosis. *N. Engl. J. Med.* **380**, 94–96 (2019).
2. L. Richeldi, H. R. Collard, M. G. Jones, Idiopathic pulmonary fibrosis. *Lancet* **389**, 1941–1952 (2017).
3. R. J. Allen, J. M. Oldham, D. A. Jenkins, O. C. Leavy, B. Guillen-Guio, C. A. Melbourne, S.-F. Ma, J. Jou, J. S. Kim; CleanUP-IPF Investigators of the Pulmonary Trials Cooperative, W. A. Fahy, E. Oballa, R. B. Hubbard, V. Navaratnam, R. Braybrooke, G. Saini, K. M. Roach, M. D. Tobin, N. Hirani, M. K. B. Whyte, N. Kaminski, Y. Zhang, F. J. Martinez, A. L. Linderholm, A. Adegunsoye, M. E. Strek, T. M. Maher, P. L. Molyneaux, C. Flores, I. Noth, R. G. Jenkins, L. V. Wain, Longitudinal lung function and gas transfer in individuals with idiopathic pulmonary fibrosis: A genome-wide association study. *Lancet Respir. Med.* **11**, 65–73 (2023).
4. M. Funke-Chambour, S. A. Guler, T. Geiser, A. Christe, J. Heverhagen, A. Pöllinger, A. Huber, L. Ebner, New radiological diagnostic criteria: Impact on idiopathic pulmonary fibrosis diagnosis. *Eur. Respir. J.* **54**, 1900905 (2019).
5. A. Sundarakrishnan, Y. Chen, L. D. Black, B. B. Aldridge, D. L. Kaplan, Engineered cell and tissue models of pulmonary fibrosis. *Adv. Drug Deliv. Rev.* **129**, 78–94 (2018).
6. L. Wain, Towards genetic reclassification of idiopathic pulmonary fibrosis. *Lancet Respir. Med.* **6**, 569–570 (2018).
7. J. A. Kropski, T. S. Blackwell, Progress in understanding and treating idiopathic pulmonary fibrosis. *Annu. Rev. Med.* **70**, 211–224 (2019).
8. P. Couvreur, Nanoparticles in drug delivery: Past, present and future. *Adv. Drug Deliv. Rev.* **65**, 21–23 (2013).
9. Q. Ji, J. Hou, X. Yong, G. Gong, M. Muddassir, T. Tang, J. Xie, W. Fan, X. Chen, Targeted dual small interfering ribonucleic acid delivery via non-viral polymeric vectors for pulmonary fibrosis therapy. *Adv. Mater.* **33**, e2007798 (2021).
10. X. Chang, L. Xing, Y. Wang, T.-J. Zhou, L.-J. Shen, H.-L. Jiang, Nanoengineered immunosuppressive therapeutics modulating M1/M2 macrophages into the balanced status for enhanced idiopathic pulmonary fibrosis therapy. *Nanoscale* **12**, 8664–8678 (2020).
11. M.-Y. Yang, Y.-J. Lin, M.-M. Han, Y.-Y. Bi, X.-Y. He, L. Xing, J.-H. Jeong, T.-J. Zhou, H.-L. Jiang, Pathological collagen targeting and penetrating liposomes for idiopathic pulmonary fibrosis therapy. *J. Control Release* **351**, 623–637 (2022).
12. H. Keum, J. Kim, D. Yoo, T. W. Kim, C. Seo, D. Kim, S. Jon, Biomimetic lipid nanocomplexes incorporating STAT3-inhibiting peptides effectively infiltrate the lung barrier and ameliorate pulmonary fibrosis. *J. Control. Release* **332**, 160–170 (2021).
13. Q. Dai, S. Wilhelm, D. Ding, A. M. Syed, S. Sindhwani, Y. Zhang, Y. Y. Chen, P. MacMillan, W. C. W. Chan, Quantifying the ligand-coated nanoparticle delivery to cancer cells in solid tumors. *ACS Nano* **12**, 8423–8435 (2018).

14. X. Chang, L. Xing, Y. Wang, C. X. Yang, Y.-J. He, T.-J. Zhou, X. D. Gao, L. Li, H. P. Hao, H.-L. Jiang, Monocyte-derived multipotent cell delivered programmed therapeutics to reverse idiopathic pulmonary fibrosis. *Sci. Adv.* **6**, eaba3167 (2020).
15. A. L. Mora, M. Rojas, A. Pardo, M. Selman, Emerging therapies for idiopathic pulmonary fibrosis, a progressive age-related disease. *Nat. Rev. Drug Discov.* **16**, 755–772 (2017).
16. C. Yao, X. Guan, G. Carraro, T. Parimon, X. Liu, G. Huang, A. Mulay, H. J. Soukiasian, G. David, S. S. Weigt, J. A. Belperio, P. Chen, D. Jiang, P. W. Noble, B. R. Stripp, Senescence of alveolar type 2 cells drives progressive pulmonary fibrosis. *Am. J. Respir. Crit. Care Med.* **203**, 707–717 (2021).
17. J. Liang, G. Huang, X. Liu, F. Taghavifar, N. Liu, Y. Wang, N. Deng, C. Yao, T. Xie, V. Kulur, K. Dai, A. Burman, S. C. Rowan, S. S. Weigt, J. Belperio, B. Stripp, W. C. Parks, D. Jiang, P. W. Noble, The ZIP8/SIRT1 axis regulates alveolar progenitor cell renewal in aging and idiopathic pulmonary fibrosis. *J. Clin. Invest.* **132**, e157338 (2022).
18. L. Hecker, N. J. Logsdon, D. Kurundkar, A. Kurundkar, K. Bernard, T. Hock, E. Melrum, Y. Y. Sanders, V. J. Thannickal, Reversal of persistent fibrosis in aging by targeting Nox4-Nrf2 redox imbalance. *Sci. Transl. Med.* **6**, 231ra47 (2014).
19. J. Xue, Z. Zhao, L. Zhang, L. Xue, S. Shen, Y. Wen, Z. Wei, L. Wang, L. Kong, H. Sun, Q. Ping, R. Mo, C. Zhang, Neutrophil-mediated anticancer drug delivery for suppression of post-operative malignant glioma recurrence. *Nat. Nanotechnol.* **12**, 692–700 (2017).
20. H. Aghajanian, T. Kimura, J. G. Rurik, A. S. Hancock, M. S. Leibowitz, L. Li, J. Scholler, J. Monslow, A. Lo, W. Han, T. Wang, K. Bedi, M. P. Morley, R. A. L. Saldana, N. A. Bolar, K. McDaid, C. A. Assenmacher, C. L. Smith, D. Wirth, C. H. June, K. B. Margulies, R. Jain, E. Puré, S. M. Albelda, J. A. Epstein, Targeting cardiac fibrosis with engineered T cells. *Nature* **573**, 430–433 (2019).
21. S. W. Wong, C. R. Tamatam, I. S. Cho, P. T. Toth, R. Bargi, P. Belvitch, J. C. Lee, J. Rehman, S. P. Reddy, J.-W. Shin, Inhibition of aberrant tissue remodelling by mesenchymal stromal cells singly coated with soft gels presenting defined chemomechanical cues. *Nat. Biomed. Eng.* **6**, 54–66 (2022).
22. O. K.-F. Ma, K. H. Chan, Immunomodulation by mesenchymal stem cells: Interplay between mesenchymal stem cells and regulatory lymphocytes. *World J. Stem Cells* **8**, 268–278 (2016).
23. J. Wu, D. Song, Z. Li, B. Guo, Y. Xiao, W. Liu, L. Liang, C. Feng, T. Gao, Y. Chen, Y. Li, Z. Wang, J. Wen, S. Yang, P. Liu, L. Wang, Y. Wang, L. Peng, G. N. Stacey, Z. Hu, G. Feng, W. Li, Y. Huo, R. Jin, N. Shyh-Chang, Q. Zhou, L. Wang, B. Hu, H. Dai, J. Hao, Immunity-and-matrix-regulatory cells derived from human embryonic stem cells safely and effectively treat mouse lung injury and fibrosis. *Cell Res.* **30**, 794–809 (2020).
24. R. L. Toonkel, J. M. Hare, M. A. Matthay, M. K. Glassberg, Mesenchymal stem cells and idiopathic pulmonary fibrosis. Potential for clinical testing. *Am. J. Respir. Crit. Care Med.* **188**, 133–140 (2013).
25. E. El Agha, R. Kramann, R. K. Schneider, X. Li, W. Seeger, B. D. Humphreys, S. Bellusci, Mesenchymal stem cells in fibrotic disease. *Cell Stem Cell* **21**, 166–177 (2017).
26. A. Zinger, L. Koren, O. Adir, M. Poley, M. Alyan, Z. Yaari, N. Noor, N. Krinsky, A. Simon, H. Gibori, M. Krayem, Y. Mumblat, S. Kasten, S. Ofir, E. Fridman, N. Milman, M. M. Lübtow, L. Liba, J. Shklover, J. Shainsky-Roitman, Y. Binenbaum, D. Hershkovitz, Z. Gil, T. Dvir, R. Luxenhofer, R. Satchi-Fainaro, A. Schroeder, Collagenase nanoparticles enhance the penetration of drugs into pancreatic tumors. *ACS Nano* **13**, 11008–11021 (2019).
27. L.-F. Zhang, X.-H. Wang, C.-L. Zhang, J. Lee, B.-W. Duan, L. Xing, L. Li, Y. K. Oh, H. L. Jiang, Sequential nano-penetrators of capillarized liver sinusoids and extracellular matrix barriers for liver fibrosis therapy. *ACS Nano* **16**, 14029–14042 (2022).
28. Q.-Q. Fan, C.-L. Zhang, J.-B. Qiao, P.-F. Cui, L. Xing, Y.-K. Oh, H.-L. Jiang, Extracellular matrix-penetrating nanodrill micelles for liver fibrosis therapy. *Biomaterials* **230**, 119616 (2020).
29. J. Weckerle, S. Picart-Armada, S. Klee, T. Bretschneider, A. H. Luippold, W. Rist, C. Haslinger, H. Schlüter, M. J. Thomas, B. Krawczyk, F. Fernandez-Albert, M. Kästle, D. Veyel, Mapping the metabolomic and lipidomic changes in the bleomycin model of pulmonary fibrosis in young and aged mice. *Dis. Model. Mech.* **15**, dmm049105 (2022).
30. F. Chua, J. Gauldie, G. J. Laurent, Pulmonary fibrosis: Searching for model answers. *Am. J. Respir. Cell Mol. Biol.* **33**, 9–13 (2005).
31. P. Kolb, C. Upagupta, M. Vierhout, E. Ayaub, P. S. Bellaye, J. Gauldie, C. Shimbori, M. Inman, K. Ask, M. R. J. Kolb, The importance of interventional timing in the bleomycin model of pulmonary fibrosis. *Eur. Respir. J.* **55**, 1901105 (2020).
32. H. Ma, X. Wu, Y. Li, Y. Xia, Research progress in the molecular mechanisms, therapeutic targets, and drug development of idiopathic pulmonary fibrosis. *Front. Pharmacol.* **13**, 963054 (2022).
33. A. F. Anvari-Yazdi, K. Tahermanesh, S. M. M. Hadavi, T. Talaei-Khozani, M. Razmkhah, S. M. Abed, M. S. Mohtasebi, Cytotoxicity assessment of adipose-derived mesenchymal stem cells on synthesized biodegradable Mg-Zn-Ca alloys. *Mater. Sci. Eng. C Mater. Biol. Appl.* **69**, 584–597 (2016).
34. A. Andrzejewska, S. Dabrowska, B. Lukomska, M. Janowski, Mesenchymal stem cells for neurological disorders. *Adv. Sci.* **8**, 2002944 (2021).
35. X. Yin, H. Tsukaya, A pulse-chase strategy for EdU labelling assay is able to rapidly quantify cell division orientation. *New Phytol.* **211**, 1462–1469 (2016).
36. R. Tian, Y. Zhu, J. Yao, X. Meng, J. Wang, H. Xie, R. Wang, NLRP3 participates in the regulation of EMT in bleomycin-induced pulmonary fibrosis. *Exp. Cell Res.* **357**, 328–334 (2017).
37. L. Li, Y. Xu, S. Li, X. Zhang, H. Feng, Y. Dai, J. Zhao, T. Yue, Molecular modeling of nanoplastic transformations in alveolar fluid and impacts on the lung surfactant film. *J. Hazard. Mater.* **427**, 127872 (2022).
38. J. F. Lewis, R. Veldhuizen, F. Possmayer, W. Sibbald, J. Whitsett, R. Qanbar, L. McCaig, Altered alveolar surfactant is an early marker of acute lung injury in septic adult sheep. *Am. J. Respir. Crit. Care Med.* **150**, 123–130 (1994).
39. M. J. Schafer, T. A. White, K. Iijima, A. J. Haak, G. Ligresti, E. J. Atkinson, A. L. Oberg, J. Birch, H. Salmonowicz, Y. Zhu, D. L. Mazula, R. W. Brooks, H. Fuhrmann-Stroissnigg, T. Pirtskhalava, Y. S. Prakash, T. Tchkonia, P. D. Robbins, M. C. Aubry, J. F. Passos, J. L. Kirkland, D. J. Tschumperlin, H. Kita, N. K. LeBrasseur, Cellular senescence mediates fibrotic pulmonary disease. *Nat. Commun.* **8**, 14532 (2017).
40. D. J. Lederer, F. J. Martinez, Idiopathic pulmonary fibrosis. *N. Engl. J. Med.* **378**, 1811–1823 (2018).
41. A. W. Wong, C. J. Ryerson, S. A. Guler, Progression of fibrosing interstitial lung disease. *Respir. Res.* **21**, 32 (2020).
42. T. Huang, T. Zhang, X. Jiang, A. Li, Y. Su, Q. Bian, H. Wu, R. Lin, N. Li, H. Cao, D. Ling, J. Wang, Y. Tabata, Z. Gu, J. Gao, Iron oxide nanoparticles augment the intercellular mitochondrial transfer-mediated therapy. *Sci. Adv.* **7**, eabj0534 (2021).
43. M. F. Pittenger, D. E. Discher, B. M. Péault, D. G. Phinney, J. M. Hare, A. I. Caplan, Mesenchymal stem cell perspective: Cell biology to clinical progress. *NPJ Regen. Med.* **4**, 22 (2019).
44. W. Zhang, M. Wang, W. Tang, R. Wen, S. Zhou, C. Lee, H. Wang, W. Jiang, I. M. Delahunty, Z. Zhen, H. Chen, M. Chapman, Z. Wu, E. W. Howerth, H. Cai, Z. Li, J. Xie, Nanoparticle-laden macrophages for tumor-tropic drug delivery. *Adv. Mater.* **34**, e2109925 (2022).
45. E. Sulheim, H. Baghirov, E. Haartman, A. Bøe, A. K. O. Åslund, Y. Mørch, C. L. Davies, Cellular uptake and intracellular degradation of poly (alkyl cyanoacrylate) nanoparticles. *J. Nanobiotechnology* **14**, 1 (2016).
46. X. Chen, A. Nomani, N. Patel, F. S. Nouri, A. Hatefi, Bioengineering a non-genotoxic vector for genetic modification of mesenchymal stem cells. *Biomaterials* **152**, 1–14 (2018).
47. G. Izbicki, M. J. Segel, T. G. Christensen, M. W. Conner, R. Breuer, Time course of bleomycin-induced lung fibrosis. *Int. J. Exp. Pathol.* **83**, 111–119 (2002).
48. L. A. Ortiz, F. Gambelli, C. McBride, D. Gaupp, M. Baddoo, N. Kaminski, D. G. Phinney, Mesenchymal stem cell engraftment in lung is enhanced in response to bleomycin exposure and ameliorates its fibrotic effects. *Proc. Natl. Acad. Sci. U.S.A.* **100**, 8407–8411 (2003).
49. M. Ono, S. Ohkouchi, M. Kanehira, N. Tode, M. Kobayashi, M. Ebina, T. Nukiwa, T. Irokawa, H. Ogawa, T. Akaike, Y. Okada, H. Kurosawa, T. Kikuchi, M. Ichinose, Mesenchymal stem cells correct inappropriate epithelial-mesenchyme relation in pulmonary fibrosis using stanniocalcin-1. *Mol. Ther.* **23**, 549–560 (2015).
50. L. Sun, M. Fan, D. Huang, B. Li, R. Xu, F. Gao, Y. Chen, Clodronate-loaded liposomal and fibroblast-derived exosomal hybrid system for enhanced drug delivery to pulmonary fibrosis. *Biomaterials* **271**, 120761 (2021).

Acknowledgments

Funding: This work was financially supported by the National Key R&D Program of China (2022YFE0198400), National Natural Science Foundation of China (82020108029 and 82073398), Project of State Key Laboratory of Natural Medicines, China Pharmaceutical University (SKLNMZZ202021), Double First-Class University Projects (CPU2018GY06), and Double First-Rate Construction Plan of China Pharmaceutical University (CPU2022QZ18).

Author contributions: H.-L.J. and M.-M.H.: Formulation or evolution of overarching research goals and aims. M.-M.H., X.-Y.H., and L.T.: Conducting a research and investigation process, specifically performing the experiments, or data collection. L.Q., M.-Y.Y., and Y.W.: Preparation, creation, and/or presentation of the published work, specifically data presentation. M.-M.H.: Preparation and presentation of the published work, specifically writing the initial draft. H.-L.J., L.X., and J.-H.J.: Oversight and leadership responsibility for the research activity planning and execution. **Competing interests:** The authors declare that they have no competing interests. **Data and materials availability:** All data needed to evaluate the conclusions in the paper are present in the paper and/or the Supplementary Materials.

Submitted 4 January 2023
Accepted 16 June 2023
Published 19 July 2023
10.1126/sciadv.adg5358